Title

Early microcystin-LR exposure-linked inflammasome activation in mice causes development of fatty liver disease and insulin resistance

Authors

Al-Badrani, Muayad
Saha, Punnag
Mondal, Ayan
et al.

Publication Date

2020-11-01

DOI

10.1016/j.etap.2020.103457

Peer reviewed

Published in final edited form as:
Environ Toxicol Pharmacol. 2020 November ; 80: 103457. doi:10.1016/j.etap.2020.103457.

Early Microcystin-LR exposure-linked inflammasome activation in mice causes development of fatty liver disease and insulin resistance

Muayad Al-Badrani[1,**,#], **Punnag Saha**[1,#], **Ayan Mondal**[1], **Ratanesh K Seth**[1], **Sutapa Sarkar**[1], **Diana Kimono**[1], **Dipro Bose**[1], **Dwayne E. Porter**[2], **Geoff I. Scott**[2], **Bryan Brooks**[3], **Samir Raychoudhury**[4], **Mitzi Nagarkatti**[5], **Prakash Nagarkatti**[5], **Saurabh Chatterjee**[1,2,*]

[1]Environmental Health and Disease Laboratory, Department of Environmental Health Sciences, Arnold School of Public Health, University of South Carolina, Columbia, SC, USA

[2]NIEHS Center for Oceans and Human Health on Climate Change Interactions, Department of Environmental Health Sciences, University of South Carolina

[3]Department of Environmental Science, Baylor University, Waco, TX 76798-7266

[4]Department of Biology, Chemistry, and Environmental Health Science, Benedict College, Columbia, SC 29204, USA.

[5]Department of Pathology, Microbiology and Immunology, University of South Carolina School of Medicine, Columbia, SC, USA

Abstract

Evidence from pediatric studies show that infants and children are at risk for early exposure to microcystin. The present report tests the hypothesis that early life exposure to microcystin (MC), a

[*]**Corresponding Author:** Dr. Saurabh Chatterjee, Associate Professor and Director, Environmental Health and Disease Lab, Environmental Health Sciences, Project Director, Toxicology Core, Center for Oceans and Human Health Center on Climate Change Interactions (OHHC2I), Adjunct Associate Professor, Department of Cell Biology and Anatomy, USC School of Medicine, University of South Carolina Research Health Scientist, Columbia VA Medical Center, Columbia, SC, schatt@mailbox.sc.edu, Ph: office: 8037778120, cell phone: 9195992278, Schatt@mailbox.sc.edu, Ph: 8037778120.
[#]Muayad Albadrani and Punnag Saha contributed equally
[**]Department of Family and Community Medicine, College of Medicine, Taibah University, Madinah, Saudi Arabia

AUTHOR CONTRIBUTIONS:
S.C. and G.I.S. conceived research, S.C. designed research; M.A., P.S., A.M., R.S., S.S., D.K., D.B. conducted experiments; S.C., M.A., P.S., A.M., R.S. analyzed data; S.C., M.A., P.S., A.M. interpreted results of the experiments; M.A., P.S., A.M., and S.C. prepared figures; M.A., P.S., S.C. drafted manuscript; D.E.P., G.I.S., B.B., S.R., M.N., P.N. edited manuscript; S.C., edited, revised, and approved final version of manuscript.

Credit author statement
Saurabh Chatterjee and Geoff I Scott: Conceptualization, **Muayad Albadrani, Punnag Saha, Ayan Mondal, Ratanesh K Seth, Sutapa Sarkar, Diana Kimono, Dipro Bose, and Saurabh Chatterjee:** Methodology; **Muayad Albadrani, Punnag Saha, Ayan Mondal, Ratanesh K Seth, Sutapa Sarkar, Diana Kimono, Dipro Bose:** Investigation; **Ayan Mondal, Ratanesh K Seth; Sutapa Sarkar**: Software: Data curation; **Saurabh Chatterjee and Muayad Albadrani** Writing- Original draft preparation; **Saurabh Chatterjee:** Visualization and supervision; **Dwayne E. Porter, Geoff I. Scott, Bryan Brooks, Samir Raychoudhury, Mitzi Nagarkatti, Prakash Nagarkatti**: Writing-Reviewing and Editing

CONFLICT OF INTERESTS:
The authors declare that there is no conflict of financial or competing interests.

principal component of harmful algal blooms followed by a juvenile exposure to high-fat diet feeding potentiate the development of nonalcoholic fatty liver disease phenotype in adulthood. Results showed classical symptoms of early NAFLD linked inflammation. Cytokines and chemokines such as CD68, IL1β, MCP-1, and TNF-α, as well as α-SMA were increased in the groups that were exposed to MC-LR with the high-fat diet compared to the vehicle group. Also, mechanistically, NLRP3 KO mice showed a significant decrease in the inflammation and NAFLD phenotype and resisted the metabolic changes such as insulin resistance and glucose metabolism in the liver. The data suggested that MC-LR exposure and subsequent NLRP3 inflammasome activation in childhood could impact liver health in juveniles.

Graphical Abstract

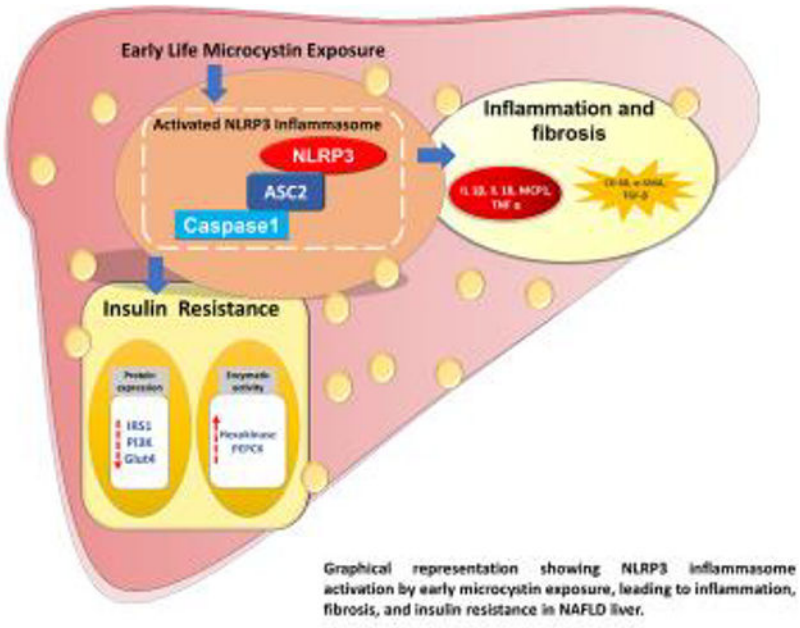

Graphical representation showing NLRP3 inflammasome activation by early microcystin exposure, leading to inflammation, fibrosis, and insulin resistance in NAFLD liver.

Keywords

Microcystin; MC-LR; NLRP3; inflammasome; PEPCK; Hexokinase; Glut4; IRS

INTRODUCTION

Microcystins, toxins found in cyanobacterial blooms of surface waters are detected worldwide (Funari and Testai, 2008). Microcystins pose a strong risk of disease development in humans through drinking water. Drinking water has been reported to be contaminated by microcystin in many regions of the world where there have been episodes of harmful algal bloom (Mohamed, 2008), (Zhou et al., 2002).

Microcystin-LR (MC-LR) is known to be the most common sub-type among other microcystins. It is primarily produced by the cyanobacterium *Microcystis aeruginosa* in the aquatic environment and is a well-known hepatotoxin (Dawson, 1998). Mechanistically, MC-LR acts as the protein phosphatase inhibitor, especially it prevents catalytic activity of

Ser/Thr protein phosphatase 1(PP1) and protein phosphatase 2A (PP2A) (MacKintosh et al., 1990), (Honkanen et al., 1990), (Xing et al., 2006). PP2A is responsible for maintaining balance of major cellular functions including cell-cycle regulation, cellular development, tumor suppression and signal transduction (Reynhout and Janssens, 2019). MC-LR binds to the catalytic subunit of PP2A covalently and diminishes catalytic activity of PP2A (Xing et al., 2006). Decreased catalytic activity of the major dephosphorylating enzyme PP2A alters the normal cellular activities and regulation of signal transductions and even may lead to tumorigenesis.

Early childhood exposure to environmental toxins has the potential to have long-life effects on individuals when they grow to adulthood. According to the American Academy of Pediatrics, infants and children are at elevated risk for early exposure to MC-LR, a constituent of harmful algal blooms. Infants and children have been known to consume more water relative to their body weight when compared to adults and thus can incur higher risks to exposure from water-borne toxins such as MC-LR. For example, the mean intake for water in infants and children is around 43 and 35 ml/kg/day, respectively. These values decrease when children are in their teen and adult ages, where they have the mean water intake of 18 and 19 ml/kg/day, respectively (Selevan et al., 2000). Also, children may be at the risk from exposure to coastal harmful algal blooms during any recreational purpose such as near ponds and beach shores.

Several studies have also established that the tissues and organs of the body undergo fast development during fetal life as well as early infancy, during which any sort of toxic insult can have significant impacts (Osmond and Barker, 2000), (Andra et al., 2015). From the progenitor cell in the fetus, the liver grows into a well-differentiated organ in which bile secretion can be started through 12 weeks gestation. It requires up to two years to reach full maturity after birth to perform complete liver function (Beath, 2003).

Obesity is considered as an epidemic and it is largely associated with numerous health problems including cardio-vascular diseases, diabetes, hypertension and NAFLD (non-alcoholic fatty liver disease). Childhood NAFLD, as a progressive result of early life high-fat diet consumption, may persist till adulthood leading to numerous pathological conditions including NASH (non-alcoholic steatohepatitis). Environmental factors like MC-LR and genetic factors often act as a “second hit” to the diet-induced metabolically reprogrammed NAFLD state. Previously we have shown that, MC-LR exposure acts as a major contributing factor in diet-induced NAFLD pathology and leads to activation of NADPH oxidase 2 (NOX2) mediated mir21 activation ((Albadrani et al., 2019)). We have also reported in our previous studies that the activation of nucleotide-binding domain-like receptor protein 3 (NLRP3) plays an active role in inflammasome activation in dysbiosis associated with non-alcoholic fatty liver disease (NAFLD) conditions following MC-LR exposure (Sarkar et al., 2019). NLRP3 inflammasome is a multi-protein complex that resides inside the cell structure (Swanson et al., 2019). It has different parts that include the cytoplasmic receptor NLRP3, which is also known as the inflammasome sensor molecule, the adaptor protein caspase-recruitment domain apoptosis-associated speck-like protein containing a CARD 2 (ASC-2) and the effector protein pro-caspase 1. Upon activation, these parts are assembled to yield several pro-caspase sub-units close to each other. This pro-caspase 1, when in

proximity within cytosolic multimolecular complexes, cleave themselves to release the mature or active form of caspase 1. The activated caspase-1 further cleaves the pro-interleukin-1β (pro-IL-1β) as well as pro-interleukin-18 (pro-IL-18) into their mature interleukin forms IL-1β and IL-18 to be released into the system (Fink and Cookson, 2005), (Agostini et al., 2004), (Kanneganti et al., 2006), (Mariathasan et al., 2006).

The activation of NLRP3 inflammasome and prolonged release of the inflammatory cytokines like IL-1β and IL-18 mediates obesity and insulin resistance (Vandanmagsar et al., 2011), (Stienstra et al., 2011). In cases of homeostatic insulin signaling, circulatory insulin binds to the insulin receptor (IR), which upon binding with insulin activates itself by autophosphorylation of the tyrosine residues. Activated IR then phosphorylates downstream insulin receptor substrates (IRS) at their multiple tyrosine residues. The phosphorylation of IRS by IR causes activation of downstream phosphoinositide 3-kinase (PI3K)- protein kinase B/Akt pathway, which in turn regulates various substrates including activating glucose uptake via AS160 (Akt substrate of 160 kDa) /TBC1D4 (TBC1 domain family member 4); elevating glycogen synthesis by deactivating GSK-3 (Glycogen synthase kinase 3) activity; inhibiting gluconeogenesis by deactivation of FOXO (Forkhead box protein) transcription factor(Yang et al., 2018). Under insulin-resistant pathology, the normal signaling pathway is altered, which affects the normal physiological regulation of these proteins and transcriptional factors, ultimately resulting in a decrease in glucose transport, glycogen synthesis and increased gluconeogenesis pathway and apoptosis (Boucher et al., 2014; Yang et al., 2018), (Siddle, 2011).

In the present study, we used a juvenile mice model primed with MC-LR followed by either co-exposing them with a lean or high-fat diet, a common mode of dietary behavior in the western world. We tested the hypothesis that early MC-LR exposure triggered the NLRP3 inflammasome activation thus creating a low inflammatory trigger that potentiates inflammation, NAFLD like outcomes and altered metabolic reprogramming in the adult liver. Also, we investigated whether the activation of the NLRP3 inflammasome may lead to an insulin-resistant like phenotype in the juvenile MC-LR primed diet-induced obesity phenotype.

MATERIALS AND METHODS

Materials

Microcystin (MC-LR) was purchased from Cayman Chemical Company (Ann Arbor, MI). Anti-CD68, anti-α-SMA, anti-3 nitrotyrosine (3NT), anti-TGF-β primary antibodies and HRP- conjugated rabbit and mouse secondary antibodies were purchased from Abcam (Cambridge, MA). Anti-GLUT 4, anti-NLRP3, anti-ASC2, anti-IL-1β and anti-β-actin primary antibodies were purchased from Santacruz Biotechnology (Dallas, TX). Anti-IRS1, anti-IRS2, anti-PI3K primary antibodies were purchased from Cell Signaling Technology (Danvers, MA) and anti-IL18 primary antibody was purchased from Abclonal (Woburn, MA). Species-specific (mouse and rabbit) biotinylated conjugated secondary antibody and streptavidin-horseradish peroxidase were purchased from Vector Laboratories (Vectastain Elite ABC kit, Burlingame, CA). Fluorescence-conjugated (Alexa Flour) secondary antibodies, ProLong Gold antifade mounting media with DAPI were purchased from

Thermofisher Scientific (Grand Island, NY). NovaUltra Special Stain Kits, applied for Picrosirius red staining was purchased from the IHC world (Woodstock, MD). Paraffin-embedding of the liver tissue sections on slides were done by AML laboratories (Baltimore, MD). All other chemicals which were used in the current study were purchased from Sigma unless otherwise specified.

Mouse model

Pathogen-free, juvenile, male (C57BL/6J) wild type (WT) and NLRP3 knock out (NLRP3 KO) mice were purchased from the Jackson Laboratories (Bar Harbor, ME) and were used for the study.

Experimental Models Used

The groups used for the experiments were (a) wild type mice fed with chow diet only (Lean), (b) wild type mice fed with chow diet and exposed to MC-LR (Lean+MC), (c) wild type mice fed with a high-fat diet (60% kCal) (HFD), (Research diets, New Brunswick, NJ) (DIO), (d) wild type mice fed with HFD and exposed to MC-LR (DIO+MC), and finally (e) NLRP3 KO exposed to MC-LR and fed with HFD (NLRP3 KO+MC). Mice were exposed to MC-LR (10μg/Kg body weight) through the intraperitoneal (i.p) route with vehicle (ethanol and PBS) starting at the age of 4 weeks. Exposure of MC-LR was continued for 2 weeks (5 dosages / week). After completion of MC-LR exposure, a group of mice was fed with HFD (DIO+ MC) and another group was fed with chow diet (Lean+MC) for the subsequent 4 weeks. Similarly, a group of mice unexposed to MC-LR, was fed with chow diet (Lean) and another with HFD diet (DIO) respectively for subsequent 4 weeks. NLRP3 KO mice group were also exposed to MC-LR for 2 weeks, followed by HFD feeding for 4 weeks (NLRP3 KO+MC). All mice groups were housed with 3 mice/cage at 23–24°C on a 12:12-h light-dark cycle with ad libitum access to food and water. The total number of animals in each group were assessed based on the calculations that ensured enough statistical power of 0.5. There were 6 mice per group (n=6) and were allocated to their respective cages following the procedure of randomization. All mice were euthanized at the age of 10 weeks after completion of the diet regime; blood serum and liver tissues were collected for further processing. Liver tissue sections were collected and fixed in 10% neutral buffered formalin after euthanization. All animals have been treated in strict accordance with the NIH Guide for the Humane Care and Use of Laboratory Animals, and the experiments were approved by the institutional review board at the University of South Carolina at Columbia. A schematic representation of all the mice treatment groups is given below.

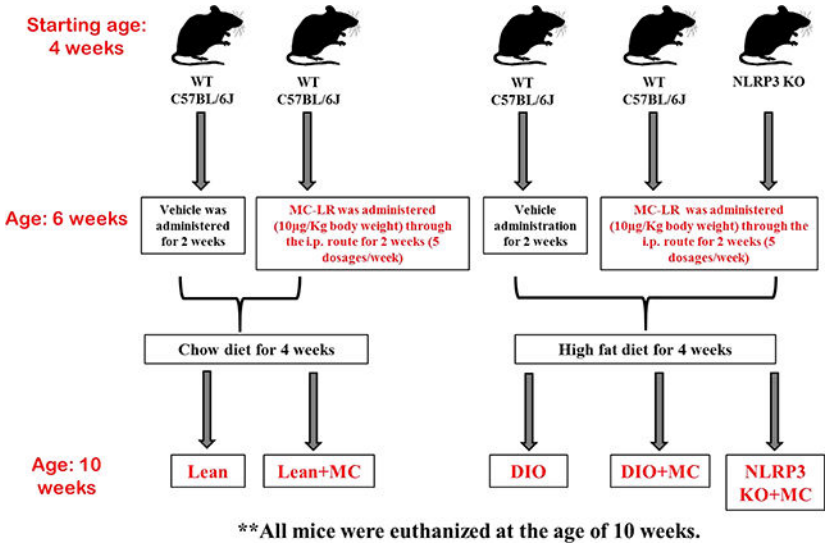

**All mice were euthanized at the age of 10 weeks.

Histopathology

Formalin-Fixed Paraffin-Embedded (FFPE) liver tissues were cut into 5 μm thick sections. For histological examinations, liver sections slides were deparaffinized using a standard protocol and stained with hematoxylin and eosin (H&E). Picrosirius red staining was performed to study collagen fiber deposition using NovaUltra Special Stain Kits following manufacturer's protocol (IHC world, Woodstock, MD) and observed under the light microscope using 20X objective.

Serum ALT Measurement

Serum alanine aminotransferase (ALT) levels were quantified and measured using an automated analyzer at the University of Georgia Clinical pathology core facility.

Serum Insulin Measurement

Serum insulin was measured using an ELISA kit (Crystal Chem, Elk Grove Village IL, USA) following the manufacturer protocol.

Immunohistochemistry

Formalin-fixed, paraffin-embedded liver tissue sections were deparaffinized using standard laboratory protocol. Epitope retrieval solution and steamer (IHC-World, Woodstock, MD, USA) were used for antigen epitope retrieval of the tissue sections. 3% H_2O_2 solution was used to block the endogenous peroxidase activity for 20 minutes, followed by serum blocking (5% goat serum, 1hr). Sections were incubated overnight at 4°C with primary antibodies for CD68, TGF-β, 3-NT, and IL-1β as recommended dilutions (1:300 in blocking buffer) in a humidified chamber. Species-specific biotinylated secondary antibody and streptavidin-conjugated with horseradish peroxidase were used according to the manufacturer's standard protocols. Finally, 3,3 diaminobenzidine (DAB) (Sigma-Aldrich) was used as a chromogenic substrate and counter stained with Mayer's hematoxylin (Sigma-Aldrich). Tissue sections were washed with 1X PBS-T (PBS+ 0.05% Tween 20) between the steps. Sections were finally mounted in Simpo mount (GBI Laboratories, Mukilteo, WA)

and observed under a 20X objective using an Olympus BX43 microscope (Olympus, America). Morphometric analysis was done using cellSens Software from Olympus America (Center Valley, PA).

Immunofluorescence Microscopy

Formalin-fixed, paraffin-embedded liver tissue sections were subjected to deparaffinization according to standard instructions. Epitope retrieval of the deparaffinized tissue sections was done with an epitope retrieval solution and steamer (IHC World) according to the manufacturer's protocol. The primary antibodies for α-SMA, NLRP3, ASC2, and IL-18 were used at recommended dilutions (1:300) and kept at 4°C for overnight incubation. Species-specific anti-IgG secondary antibodies conjugated with Alexa Fluor 633 or 488 (Invitrogen, California, USA) were used. The tissue sections were mounted in a ProLong Gold antifade reagent with DAPI (Life Technologies, Carlsbad, CA). Images were captured under 40X magnification with an Olympus BX43 microscope. Morphometric analysis was done using the cellSens software.

Quantitative Real-Time Polymerase Chain Reaction

Gene expression for mRNA levels from juvenile mice liver tissue was measured by quantitative real-time reverse transcription-polymerase chain reaction (qRT-PCR) by following our routine laboratory protocol. The primers used for RT-PCR in 5′ to 3′ orientations are provided in Table 4.1.

Western blot

Proteins from respective liver tissue samples were extracted using RIPA lysis buffer and subsequently quantified by the BCA assay kit (Thermo Fisher Scientific, Rockford, IL). Approximately, 30 μg of denatured protein was loaded on per well of Novex 4%–12% bis-tris gradient gel and subjected to standard SDS-PAGE. Resolved protein bands were then transferred to a nitrocellulose membrane using the Trans-Blot Turbo transfer system (Bio-rad, Hercules, CA). After Ponceau S staining, the membrane was blocked with 5% bovine serum albumin (BSA) for 1 hour, followed by incubation with primary antibody for overnight at 4 °C. Primary antibodies against IRS-1, IRS-2, PI3K, GLUT4, and β-actin were used at recommended dilutions, and compatible horseradish peroxidase-conjugated secondary antibodies were used to tag the primary antibody. Pierce ECL Western blotting substrate (Thermo Fisher Scientific, Waltham, MA, USA) was used for the development of the blot. Finally, the blots were captured using G: Box Chemi XX6 and subjected to densitometry analysis using Image J software.

Biochemical assays for hexokinase & phosphoenolpyruvate carboxykinase activity

Hepatic intracellular hexokinase (HK) & phosphoenolpyruvate carboxykinase (PEPCK) activity were measured using Hexokinase Colorimetric Assay Kit and Phosphoenolpyruvate Carboxykinase Colorimetric Activity Assay Kit (Biovision, Milpitas, CA) respectively. All procedures were performed according to the manufacture's protocol.

Statistical Analysis

All mice experiments were repeated three times with at least 6 mice per group (n = 6) unless otherwise mentioned; data from each group of 6 mice were pooled). Data were represented as mean ± S.E. The graphs were plotted using GraphPad Software, Inc. The statistical analysis was carried out by unpaired t-test and ANOVA and significance was measured by Bonferroni Dunn post hoc correction method. For all analyses, $p < 0.05$ was considered statistically significant.

RESULTS

1. Early life exposure to microcystin in mice primes liver to a progressive non-viral hepatitis pathology

To determine the effects of early priming exposure of MC-LR in mice immediately after weaning on liver parenchyma, liver histopathology as well as inflammatory markers were analyzed. The early exposed MC-LR mice (Lean+MC) showed an increase in liver injury pathophysiology, as shown by increased infiltrating immune cells (early inflammation) when compared with Lean control mice (mice that had lean diet and are considered healthy) that were only exposed to vehicle (Fig. 1 A). Mild fibrotic pathology was significant with picrosirius red staining in MC-LR exposed mice (Fig. 1B, 1E) ($p< 0.001$). Moreover, to investigate if early priming with MC-LR can induce activation for both Kupffer cells and hepatic stellate cells, hallmarks of hepatitis pathology, immunoreactivities of Kupffer cell activation marker CD68, as well as hepatic stellate cell activation marker α-smooth muscle actin (α-SMA), were analyzed in liver tissue slices at age that depicts adulthood (10–12 weeks). Results showed that there was a significant increase in CD68 immunoreactivity in (Lean+MC) mice as compared with Lean control group of mice ($p < 0.001$) (Fig.1, C, and F and Supplementary Fig. 2). These findings have been further confirmed at the mRNA levels of CD68 as well as the inflammatory markers. CD68 mRNA expression in (Lean+MC) mice increased significantly when compared with Lean control mice ($p = 0.008$) (Fig. 1, H). Moreover, to test that the activation of Kupffer cells took part in a proinflammatory phenotype, mRNA expression of pro-inflammatory cytokines such as monocyte-chemoattractant protein-1 (MCP-1), interleukin 1 beta (IL-1β), and tumor necrosis factor-α (TNF-α) were evaluated. The result showed that there was a significant increase in MCP-1, IL-1β and TNF-α mRNA expression in (Lean+MC) mice as compared with Lean control mice ($p < 0.001$, $p= 0.005$, and $p < 0.001$, respectively) (Fig. 1, H). α-SMA immunoreactivity, a characteristic of stellate cell activation was also significantly increased in (Lean+MC) mice when compared with Lean control mice group ($p < 0.001$) (Fig. 1, D and G). α-SMA mRNA expressions in (Lean+MC) mice have increased significantly when compared with the Lean control mice group ($p < 0.001$) (Fig. 1, H). Furthermore, liver tissues were also analyzed for fibrosis status by assessing picrosirius red staining. The above results thus suggested that a childhood MC-LR exposure induced a non-viral hepatitis pathology in adulthood via increased proinflammatory responses by MCP-1, IL-1β, and TNF-α.

2. Early exposure to microcystin followed by a prolonged high-fat diet feeding (HFD) mimicking current western dietary habits and sedentary lifestyle accelerated NASH-like phenotype in adulthood

We and others have shown that toxins from the environmental exposure may act as a second hit to intensify the progression of NAFLD from early-stage to advanced inflammatory phenotype seen in nonalcoholic steatohepatitis (NASH) (Seth et al., 2013), (Nagata et al., 2007)). We have also shown previously that exogenous inhibitors of PP2A such as MC-LR can worsen the pathophysiology of NAFLD (Albadrani et al., 2019). To investigate the role of early exposure to MC-LR in the induction of liver injury in a diet-induced obesity (DIO) model, we used a low and chronic dose of MC-LR in mice immediately after weaning to induce liver injury, followed by feeding them HFD (DIO+MC). Results showed that (DIO +MC) group had all the typical features of NAFLD/NASH including increased infiltrating immune cells (inflammation) and hepatocytes ballooning when compared to DIO control mice alone, (Lean+MC) mice, or Lean control mice (Fig. 2, A). Early exposure to MC-LR also significantly elevated serum ALT levels in (DIO+MC) mice as compared to Lean control, (Lean+MC) mice and DIO only mice ($p < 0.05$) (Fig. 4A). Moreover, the analysis of picrosirius red staining in the early exposure to MC-LR followed by HFD (DIO+MC) mice group showed increased reactivity as compared to lean control, (Lean+MC) mice and DIO only mice ($p < 0.05$) (Fig. 2B and 3A). CD68 immunoreactivity, as well as mRNA levels, were significantly increased in early exposure to MC-LR followed by HFD mice in adulthood (DIO+MC) group as compared to lean control, (lean+MC) mice and DIO only mice group ($p < 0.05$) (Fig. 2C, 3B, 4B and Supplementary Fig. 2). This is indicative of Kupffer cell activation, a hallmark of development of steatohepatitis in early exposure to MC-LR followed by HFD (DIO+MC) mice group as evidenced by a significant increase in CD68. To study the effect of early MC-LR exposure in NAFLD in stellate cell proliferation, immunohistochemistry and mRNA expression of stellate cell activation marker α-SMA were studied. Transforming growth factor-beta (TGF-β) was also studied in parallel to α-SMA because it has been shown in different studies akin to our own observations that they are key to fibrogenesis in the liver (Dattaroy et al., 2015),. α-SMA, as well as TGF-β immunoreactivity and their mRNA expression levels, were significantly increased in the early exposure to MC-LR followed by HFD (DIO+MC) mice groups when compared with DIO mice, the (Lean + MC) mice group or lean control group($p < 0.001$) (Fig. 2E and 2D) (2D and 3C)(4C and 4D).

High-fat diet fed mice (DIO+MC) exposed to MC-LR in childhood also showed increased mRNA expression of proinflammatory cytokines TNF-α, IL-1β, and MCP-1 as compared to the other corresponding control groups ($p < 0.05$) (Fig. 4B). The above findings, therefore, indicated that pro-non-viral hepatitis symptoms, a phenotype resembling clinical indicators of NASH and pro-inflammatory responses via IL-1β, MCP-1 and TNF-α were induced by early MC exposure in mice that had exposure to high-fat diet feeding (DIO+MC) mice.

3. Early exposure to microcystin followed by HFD feeding induced hepatic oxidative stress via tyrosine radical formation

Oxidative stress pathway activation is one of the most important pathogenic mechanisms associated with chronic liver injury and nonalcoholic steatohepatitis (Zhang et al., 2018a),

(Mortezaee and Khanlarkhani, 2018). Evidence-based research confirms that 3-nitrotyrosine (3-NT) formation *in vivo* as well as *in vitro* occurs under various pathological conditions particularly in the liver of NASH mouse models and human subjects. 3-NT is a well-established biomarker of peroxynitrite-mediated oxidative damage in the diseased liver (Ahsan, 2013), (Dattaroy et al., 2016). Results showed that the immunoreactivity of 3-NT as analyzed by immunohistochemistry in early exposure to MC-LR followed by HFD (DIO +MC) mice groups was significantly increased compared to DIO mice, (Lean +MC) mice group or Lean control group (Figure 5A and 5B) ($p < 0.05$). This indicates that early exposure to MC-LR had a clear role in the development of tyrosine radicals and tyrosine residue nitration in the high-fat diet with early MC-LR exposure (DIO+MC) group. The oxidative stress thus caused might be an underlying mechanism that bridges pathology associated with MC-LR priming and NASH development in adulthood.

4. NASH-like pathology in adulthood following early microcystin exposure is associated with NLRP3-linked inflammasome activation

Many studies are indicating the role of NLRP3 inflammasome activation in different inflammatory hepatic pathology as a major contributor to hepatocyte damage, activation of immune cells and hepatic inflammation (Szabo and Petrasek, 2015),(Wan et al., 2016), (Wree et al., 2014), (Yang and Lim, 2014). Our group has shown previously that MC-LR can mediate peroxynitrite formation via NOX2-mediated inflammasome activation in intestinal inflammatory pathology (Sarkar et al., 2019). To investigate whether early exposure to MC-LR can result in inflammasome activation in the normal lean diet-fed and high-fat diet fed liver tissue, we measured mRNA expressions of the NLRP3 as well as ASC2 inflammasome sub-units. We also conducted dual immunofluorescent labeling to identify co-localization events of both ASC2 and NLRP3 to demonstrate efficient assembly of the inflammasome complex. Results showed that there was an increase in mRNA expression levels for NLRP3 as well as ASC2 inflammasome sub-units in the early exposed to MC-LR with HFD mice (DIO+MC) when compared to DIO mice, the (Lean + MC) mice group or Lean control group (Figure 6A–6D, Supplementary Fig. 1) ($p < 0.05$). It is known that Caspase1 mediated IL-1β, as well as IL-18 release, a hallmark of the NLRP3-mediated inflammasome activation response that is downstream of the inflammasome assembly, is strongly associated with NLRP3 inflammasome activation in Kupffer cells (Fink and Cookson, 2005), (Kelk et al., 2003). To investigate whether early exposure to MC-LR with HFD can result in the release of IL-1β and IL-18 we measured mRNA expression of the above cytokines by qRT-PCR and their immunoreactivity. Results showed increased immunoreactivity of IL-1β and IL-18 in (DIO + MC) mice groups as compared with DIO mice, the (Lean + MC) mice group or Lean control group (Figure 7 A, B, C, and D) ($p < 0.05$). Results also showed that there was an increase in mRNA expression levels for IL-1β and IL-18 genes in mice that have early exposure to MC-LR followed by HFD (DIO+MC) as compared to DIO mice, the (Lean + MC) mice group or Lean control group (Figure 7E) ($p < 0.05$). Furthermore, to investigate the role of NLRP3 inflammasome activation and its role in the subsequent development of the NAFLD phenotype, we used NLRP3 gene-deleted mice (NLRP3 KO) early exposed to MC-LR and fed with HFD (NLRP3 KO+MC). The immunohistochemistry of 3NT, a marker of peroxynitrite-induced oxidative stress, as well as Kupffer cell activation marker CD68 were performed. Results showed that there was a significantly increased

immunoreactivity of 3NT in (DIO + MC) group when compared with DIO mice alone, whereas there was a significant decrease in the above-mentioned immunoreactivities in (NLRP3 KO+MC) mice groups (p= 0.013) (Fig.8 A and 9A). Results also showed decreased immunoreactivity of CD68 in (NLRP3 KO+MC) mice group ($p < 0.001$) (Fig.8 B, 9B and Supplementary Fig. 2) when compared to (DIO+MC) group suggesting Kupffer cell activation was dependent on NLRP3 inflammasome activation. The mRNA expression of proinflammatory cytokines CD68, MCP-1, and TNF-α showed a significant increase in (DIO+MC) mice groups, whereas a decrease in (NLRP3 KO+MC) mice groups was observed ($p <0.001$) (Fig. 9G) suggesting that NLRP3 inflammasome activation was directly involved in the downstream inflammatory events in the diseased liver following MC-LR priming early in the life. Moreover, the immunoreactivity of a cytokine known for its role in fibrosis (TGF-β) using immunohistochemistry staining as well as the immunoreactivity of stellate cell activation marker (α-SMA) using immunofluorescence staining was performed. Results showed that there was a significantly increased immunoreactivity of TGF-β as well as α-SMA in (DIO+MC) mice when compared with DIO mice alone, whereas there were a significant reduction in (NLRP3 KO+MC) mice groups ($p <0.001$) (Fig.8C, 8D, 9C, and 9D). Similarly, the mRNA expression of TGF-β and α-SMA genes showed a significant increase in (DIO+MC) mice groups, whereas a decrease in (NLRP3 KO+MC) mice groups were observed in mice lacking the NLRP3 gene($p <0.001$) (Fig.10A). Caspase1 mediated IL-1β, as well as IL-18 release, also was evaluated to show a direct correlation and association of the NLRP3 gene and its subsequent assembly by using the NLRP3 KO mice. Results showed there was a significant decrease in (NLRP3 KO+MC) mice group ($p < 0.001$) (Fig.8E, 8F, 9E, 9F) when compared to (DIO+MC) group. The mRNA expression of IL-1β and IL-18 genes also showed a significant decrease in (NLRP3 KO+MC) mice groups was observed ($p <0.001$) when compared to (DIO+MC) group (Fig 10B). Thus, the data above suggested that an early MC-LR exposure activated Kupffer cells, helped to attain a myofibroblast phenotype in stellate cells, increased inflammation, and were NLRP3 inflammasome assembly dependent.

5. Early exposure to microcystin followed by HFD-feeding leads to NLRP3-dependent increases in insulin resistance, decreased hepatic expression of insulin receptor substrates (IRS), and phosphoinositide 3-kinase (PI3K)

Inflammation activation is often associated with type 2 diabetes mellitus and insulin resistance and has been extensively reviewed (Rheinheimer et al., 2017), (Ding et al., 2019). Aging-associated insulin resistance showed the involvement of NLRP3 inflammasome (He et al., 2020). In our study, we wanted to determine whether the inflammation activation can lead to a sustained insulin resistance like phenotype in the (DIO+MC) mice model that were exposed to MC-LR early in their childhood. In order to explore the detailed relationship between inflammasome activation and insulin-resistant like phenotype, serum ELISA for insulin was performed. Results showed that early MC-LR primed Lean or DIO groups had significantly elevated level of serum insulin compared to the Lean control or DIO mice group respectively ($p <0.001$) but a significantly decreased level of serum insulin was observed for (NLRP3 KO+MC) mice group (Fig. 11)($p <0.001$) compared to the (DIO+MC) group. Insulin signaling pathways consist of the binding of insulin with the insulin receptor (IR) in the hepatocytes. This receptor autophosphorylation occurs on the tyrosine residues of

IR, which further results in the phosphorylation of the insulin receptor substrates (IRS1, IRS2) and subsequently results in downstream signaling via the PI3K-Akt mediated pathway (Boucher et al., 2014). Immunoblots obtained from proteins extracted from liver tissues showed a significant decrease in the expression of IRS2 ($p < 0.01$), IRS1 ($p < 0.01$), PI3K ($p < 0.001$) in (DIO+MC) group when compared to the DIO group but no significant decrease was observed for the (NLRP3 KO+MC) mice group for PI3K and IRS1 (Fig. 12A–12D). Decreased expression of GLUT4, which acts as an insulin-dependent pathway, is a signature of insulin resistance as the cells fail to uptake glucose from the outer circulation. In our result, we observed a significantly decreased expression of GLUT4 protein in immunoblots for the (DIO+MC) group when compared to DIO group ($p < 0.001$). The change was reversed in (NLRP3 KO+MC) mice and the levels of GLUT4 were comparable to controls (Fig. 12E). This result coupled with the previous insulin signaling protein expression study clearly implicated a strong association between insulin resistance like phenotype, and the failure of glucose transport in the hepatocytes (Fig. 11 and 12). These results implicate that early exposure to MC-LR followed by HFD can alter the expression of insulin signaling pathway proteins via NLRP3 inflammasome activation which in turn may induce insulin-resistant like phenotype in the liver.

6. Early priming of Microcystin causes NLRP3-dependent increased gluconeogenesis ultimately resulting in an insulin-resistant like phenotype

Insulin-resistant cells, which fail to uptake glucose from the circulation, shift to gluconeogenesis pathway due to a lack of normal glucose in the system (Hatting et al., 2018). Metabolic studies using radioisotopes have shown that liver glycogen concentrations are reduced and the rate of hepatic gluconeogenesis is increased in subjects with type 2 diabetes; thus, the higher rate of glucose production in type 2 diabetes can be attributed entirely to increased rates of hepatic gluconeogenesis (Shulman, 1999). To study the gluconeogenesis pathway, the enzymatic activity of two rate-limiting enzymes in the pathway, hexokinase (HK) and phosphoenolpyruvate carboxykinase (PEPCK) activity were measured in the liver cells. Results showed that HK activity was significantly increased following the early priming of mice with MC-LR and co-exposure with either lean diet or high-fat diet feeding (Fig. 13A). (NLRP3 KO+MC) mice treated identically had a significant decrease in the activity of the HK enzyme suggesting that inflammasome activation had a significant role to play in the insulin-resistant liver and the gluconeogenesis that followed. A similar trend in the results was obtained for PEPCK specific activity which also plays a significant role in gluconeogenesis from lactate and pyruvate in the liver (Vogt, 1997). The PEPCK activity was increased (not significant) in the (DIO+MC) group when compared to DIO-only group however there was a significant decrease in its activity in NLRP3 gene deleted mice (NLRP3 KO+MC) group suggesting that NLRP3 had a significant role to play in the enzyme activity crucial in insulin resistance in hepatic metabolic reprogramming (Fig. 13B).

DISCUSSION

The present study reports the role of early MC-LR exposure in exacerbating liver injury outcomes that mimic a NAFLD phenotype. Moreover, this study suggests the role of the

NLRP3 inflammasome complex in the progression of a NAFLD phenotype later in life with preceding toxin exposure. The results showed that mice primed with sub-chronic doses of MC-LR for two weeks immediately after their weaning followed by a high-fat diet has increased serum ALT levels. In addition, the findings reported in this study indicate that early MC-LR exposure induced heightened inflammation, increased stellate cell activation, and early onset of fibrosis. These findings provide an enhanced argument in favor of recent pediatric epidemiology data, that report increased NAFLD prevalence among children who are overweight in comparison to healthy and non-overweight subjects. Our findings also assume relevance in clinical research where positive associations between obesity and progressions of chronic liver pathology such as NASH have been ascribed to environmental and genetic factors.

Pediatric NAFLD, common chronic liver disease in childhood and adolescence and is similar in many ways to NAFLD in adults but has been shown to have important differences in predisposition, presentation, and differential diagnosis. Importantly, antenatal and early childhood exposures and the particular vulnerabilities to environmental influences in a growing child, present unique opportunities for intervention and modification of risk (Fitzpatrick and Dhawan, 2019). Though much research has been carried out in NAFLD/NASH pathology in recent years, environmental factors that predispose subjects to fatty liver disease and their mechanistic pathways have hardly been defined. The present study is unique since it mimics a setting where early life exposure to a potential hepatotoxin increases the risk of development of hepatic insulin resistance and fatty liver phenotype. In addition, the study also identifies hepatic inflammation and metabolic reprogramming primarily through inflammasome activation as a key pathway that mediates the priming process to toxins and also paves the way for hepatic disease.

NLRP3 inflammasome, when activated, results in activation of pro-caspase1 and pro-IL-1β. That, in turn, gets converted to IL-1β, which is known to have a key role in NASH development within the NAFLD spectrum (Wan et al., 2016). Our findings of increased NLRP3 and ASC2 assembly using dual staining for co-localization proved the process of inflammasome activation following priming with MC-LR in DIO models. Subsequent to inflammasome activation, there were increases in markers of Kupffer cell activation (CD68) as well as stellate cell activation (α-SMA) in the MC-LR primed mouse liver while the same was decreased in NLRP3 KO mice. Though the data strongly indicated that inflammasome activation was a key to the development of NAFLD phenotype in adolescence, the increase in its activation following MC-LR alone in mice consuming lean diet possibly shows that MC-LR exposure had a significant role in priming the liver to metabolic disease in adolescent age (Fig. 6A and 6B).

We have shown previously that oxidative stress-mediated by peroxynitrite generation plays a central role in activating Kupffer cells during early steatohepatitis in NASH (Seth et al., 2013). We and others also have shown earlier that peroxynitrite generation in NAFLD creates a stable nitrated residue of tyrosine 3-nitrotyrosine (3NT) protein (Seth et al., 2013), (Chatterjee et al., 2013). This protein is established as a biomarker for oxidative stress in liver injury (Ahsan, 2013), (Abdelmegeed and Song, 2014). Moreover, we published data that provided mechanistic cues in MC-LR exposure that induced NASH pathology, wherein

Kupffer cells could be the key cell site for the generation of NOX2-dependent ROS. In our present study, we found an increase at the level of 3-NT in mice primed with MC-LR in DIO models while also finding a decrease of this ROS marker in NLRP3 KO mice. The above-described result is also indicative of the fact that MC-LR exposure primed increase of ROS production in the liver and an extended exposure later in life with a diet rich in fat would have exacerbated the generation of ROS further resulting in lipotoxicity and hepatic tissue damage. Our results also showed a significant increase in expression levels of α-SMA and TGF-β in mice primed with MC-LR in high-fat fed mice, while their level of expression was significantly decreased in NLRP3 KO mice. This result also correlated well with an increased picrosirius red stain in MC-LR primed mice suggesting mild fibrosis in groups with high-fat feeding while such fibrosis was decreased in NLRP3 KO mice (data not shown).

NAFLD is characterized by metabolic alterations including hepatic insulin resistance, a predominance of gluconeogenesis and increased expression of fatty acid metabolism genes SREBP1c, PPAR-γ and PPAR-α. A recent study showed that exposure to *Microcystis* bloom water containing MC-LR can induce the incidence of type 2 diabetes mellitus (T2DM), by impairing the function of mitochondria by MC-LR (Zhang et al., 2018b). Both acute and chronic exposure of MC-LR, even at very low concentrations (1 μg/L), impaired the insulin receptor signaling pathway and induced hyperinsulinemia and insulin resistance in mice (Zhang et al., 2018b). Interestingly, our results echo the above findings and shed important light on a possible scenario of likely progression of an underlying T2DM condition into full-blown steatohepatitis. In addition, our studies also provide mechanistic insight into the role of NLRP3 inflammasomes in insulin resistance, decreased glucose intake in hepatocytes following decreased protein expression of GLUT4 and the increased activity of glucogenesis enzymes.

In summary, our results clearly show that early exposure to MC-LR causes an adolescent NAFLD phenotype with hepatic insulin resistance and a preponderance of gluconeogenesis similar to advanced metabolic complications associated with NAFLD. The above report also advances our understanding of the possible risk that may be associated with drinking water or swimming in watersheds that might have microcystin levels higher than EPA permissible limits, particularly in childhood.

Supplementary Material

Refer to Web version on PubMed Central for supplementary material.

ACKNOWLEDGEMENTS

The authors gratefully acknowledge the technical services at the IRF, University of South Carolina School of Medicine and AML Labs (Baltimore MD). We also thank the Instrumentation resource facility (IRF) at the University of South Carolina for equipment usage and consulting services.

FUNDING:

This work has been supported by National Institutes of Health Awards P20-GM-103641-06, P01-ES-028942-01, and P01-AT-003961 to S. Chatterjee; 1-P01-ES-028942-01 to D.E. Porter and G. I. Scott; and P01-AT-003961, P20-GM-103641, R01-AT-006888, R01-ES-019313, R01-MH-094755 to M. Nagarkatti and P. S. Nagarkatti.

References

Abdelmegeed MA, Song BJ, 2014 Functional roles of protein nitration in acute and chronic liver diseases. Oxidative medicine and cellular longevity 2014, 149627. [PubMed: 24876909]

Agostini L, Martinon F, Burns K, McDermott MF, Hawkins PN, Tschopp J, 2004 NALP3 forms an IL-1beta-processing inflammasome with increased activity in Muckle-Wells autoinflammatory disorder. Immunity 20, 319–325. [PubMed: 15030775]

Ahsan H, 2013 3-Nitrotyrosine: A biomarker of nitrogen free radical species modified proteins in systemic autoimmunogenic conditions. Human immunology 74, 1392–1399. [PubMed: 23777924]

Albadrani M, Seth RK, Sarkar S, Kimono D, Mondal A, Bose D, Porter DE, Scott GI, Brooks B, Raychoudhury S, Nagarkatti M, Nagarkatti P, Jule Y, Diehl AM, Chatterjee S, 2019 Exogenous PP2A inhibitor exacerbates the progression of nonalcoholic fatty liver disease via NOX2-dependent activation of miR21. American journal of physiology. Gastrointestinal and liver physiology 317, G408–G428. [PubMed: 31393787]

Andra SS, Austin C, Wright RO, Arora M, 2015 Reconstructing pre-natal and early childhood exposure to multi-class organic chemicals using teeth: Towards a retrospective temporal exposome. Environment international 83, 137–145. [PubMed: 26134987]

Beath SV, 2003 Hepatic function and physiology in the newborn. Semin Neonatol 8, 337–346. [PubMed: 15001122]

Boucher J, Kleinridders A, Kahn CR, 2014 Insulin receptor signaling in normal and insulin-resistant states. Cold Spring Harb Perspect Biol 6.

Chatterjee S, Ganini D, Tokar EJ, Kumar A, Das S, Corbett J, Kadiiska MB, Waalkes MP, Diehl AM, Mason RP, 2013 Leptin is key to peroxynitrite-mediated oxidative stress and Kupffer cell activation in experimental non-alcoholic steatohepatitis. J Hepatol 58, 778–784. [PubMed: 23207144]

Dattaroy D, Pourhoseini S, Das S, Alhasson F, Seth RK, Nagarkatti M, Michelotti GA, Diehl AM, Chatterjee S, 2015 Micro-RNA 21 inhibition of SMAD7 enhances fibrogenesis via leptin-mediated NADPH oxidase in experimental and human nonalcoholic steatohepatitis. American journal of physiology. Gastrointestinal and liver physiology 308, G298–312. [PubMed: 25501551]

Dattaroy D, Seth RK, Das S, Alhasson F, Chandrashekaran V, Michelotti G, Fan D, Nagarkatti M, Nagarkatti P, Diehl AM, Chatterjee S, 2016 Sparstolonin B attenuates early liver inflammation in experimental NASH by modulating TLR4 trafficking in lipid rafts via NADPH oxidase activation. American journal of physiology. Gastrointestinal and liver physiology 310, G510–525. [PubMed: 26718771]

Dawson RM, 1998 The toxicology of microcystins. Toxicon 36, 953–962. [PubMed: 9690788]

Ding S, Xu S, Ma Y, Liu G, Jang H, Fang J, 2019 Modulatory Mechanisms of the NLRP3 Inflammasomes in Diabetes. Biomolecules 9.

Fink SL, Cookson BT, 2005 Apoptosis, pyroptosis, and necrosis: mechanistic description of dead and dying eukaryotic cells. Infect Immun 73, 1907–1916. [PubMed: 15784530]

Fitzpatrick E, Dhawan A, 2019 Childhood and Adolescent Nonalcoholic Fatty Liver Disease: Is It Different from Adults? Journal of clinical and experimental hepatology 9, 716–722. [PubMed: 31889753]

Funari E, Testai E, 2008 Human health risk assessment related to cyanotoxins exposure. Critical reviews in toxicology 38, 97–125. [PubMed: 18259982]

Hatting M, Tavares CDJ, Sharabi K, Rines AK, Puigserver P, 2018 Insulin regulation of gluconeogenesis. Annals of the New York Academy of Sciences 1411, 21–35. [PubMed: 28868790]

He M, Chiang HH, Luo H, Zheng Z, Qiao Q, Wang L, Tan M, Ohkubo R, Mu WC, Zhao S, Wu H, Chen D, 2020 An Acetylation Switch of the NLRP3 Inflammasome Regulates Aging-Associated Chronic Inflammation and Insulin Resistance. Cell metabolism 31, 580–591 e585. [PubMed: 32032542]

Honkanen RE, Zwiller J, Moore RE, Daily SL, Khatra BS, Dukelow M, Boynton AL, 1990 Characterization of microcystin-LR, a potent inhibitor of type 1 and type 2A protein phosphatases. J Biol Chem 265, 19401–19404. [PubMed: 2174036]

Kanneganti TD, Body-Malapel M, Amer A, Park JH, Whitfield J, Franchi L, Taraporewala ZF, Miller D, Patton JT, Inohara N, Nunez G, 2006 Critical role for Cryopyrin/Nalp3 in activation of caspase-1 in response to viral infection and double-stranded RNA. J Biol Chem 281, 36560–36568. [PubMed: 17008311]

Kelk P, Johansson A, Claesson R, Hanstrom L, Kalfas S, 2003 Caspase 1 involvement in human monocyte lysis induced by Actinobacillus actinomycetemcomitans leukotoxin. Infect Immun 71, 4448–4455. [PubMed: 12874324]

MacKintosh C, Beattie KA, Klumpp S, Cohen P, Codd GA, 1990 Cyanobacterial microcystin-LR is a potent and specific inhibitor of protein phosphatases 1 and 2A from both mammals and higher plants. FEBS letters 264, 187–192. [PubMed: 2162782]

Mariathasan S, Weiss DS, Newton K, McBride J, O'Rourke K, Roose-Girma M, Lee WP, Weinrauch Y, Monack DM, Dixit VM, 2006 Cryopyrin activates the inflammasome in response to toxins and ATP. Nature 440, 228–232. [PubMed: 16407890]

Mohamed ZA, 2008 Toxic cyanobacteria and cyanotoxins in public hot springs in Saudi Arabia. Toxicon 51, 17–27. [PubMed: 17825867]

Mortezaee K, Khanlarkhani N, 2018 Melatonin application in targeting oxidative-induced liver injuries: A review. J Cell Physiol 233, 4015–4032. [PubMed: 29023783]

Nagata K, Suzuki H, Sakaguchi S, 2007 Common pathogenic mechanism in development progression of liver injury caused by non-alcoholic or alcoholic steatohepatitis. J Toxicol Sci 32, 453–468. [PubMed: 18198478]

Osmond C, Barker DJ, 2000 Fetal, infant, and childhood growth are predictors of coronary heart disease, diabetes, and hypertension in adult men and women. Environmental health perspectives 108 Suppl 3, 545–553.

Reynhout S, Janssens V, 2019 Physiologic functions of PP2A: Lessons from genetically modified mice. Biochim Biophys Acta Mol Cell Res 1866, 31–50. [PubMed: 30030003]

Rheinheimer J, de Souza BM, Cardoso NS, Bauer AC, Crispim D, 2017 Current role of the NLRP3 inflammasome on obesity and insulin resistance: A systematic review. Metabolism: clinical and experimental 74, 1–9. [PubMed: 28764843]

Sarkar S, Kimono D, Albadrani M, Seth RK, Busbee P, Alghetaa H, Porter DE, Scott GI, Brooks B, Nagarkatti M, Nagarkatti P, Chatterjee S, 2019 Environmental microcystin targets the microbiome and increases the risk of intestinal inflammatory pathology via NOX2 in underlying murine model of Nonalcoholic Fatty Liver Disease. Scientific reports 9, 8742. [PubMed: 31217465]

Selevan SG, Kimmel CA, Mendola P, 2000 Identifying critical windows of exposure for children's health. Environmental health perspectives 108 Suppl 3, 451–455. [PubMed: 10852844]

Seth RK, Kumar A, Das S, Kadiiska MB, Michelotti G, Diehl AM, Chatterjee S, 2013 Environmental toxin-linked nonalcoholic steatohepatitis and hepatic metabolic reprogramming in obese mice. Toxicological sciences : an official journal of the Society of Toxicology 134, 291–303. [PubMed: 23640861]

Shulman GI, 1999 Cellular mechanisms of insulin resistance in humans. Am J Cardiol 84, 3J–10J.

Siddle K, 2011 Signalling by insulin and IGF receptors: supporting acts and new players. J Mol Endocrinol 47, R1–10. [PubMed: 21498522]

Stienstra R, van Diepen JA, Tack CJ, Zaki MH, van de Veerdonk FL, Perera D, Neale GA, Hooiveld GJ, Hijmans A, Vroegrijk I, van den Berg S, Romijn J, Rensen PC, Joosten LA, Netea MG, Kanneganti TD, 2011 Inflammasome is a central player in the induction of obesity and insulin resistance. Proceedings of the National Academy of Sciences of the United States of America 108, 15324–15329. [PubMed: 21876127]

Swanson KV, Deng M, Ting JP, 2019 The NLRP3 inflammasome: molecular activation and regulation to therapeutics. Nature reviews. Immunology 19, 477–489.

Szabo G, Petrasek J, 2015 Inflammasome activation and function in liver disease. Nature reviews. Gastroenterology & hepatology 12, 387–400. [PubMed: 26055245]

Vandanmagsar B, Youm YH, Ravussin A, Galgani JE, Stadler K, Mynatt RL, Ravussin E, Stephens JM, Dixit VD, 2011 The NLRP3 inflammasome instigates obesity-induced inflammation and insulin resistance. Nature medicine 17, 179–188.

Vogt J, 1997 Gluconeogenesis in patients with impaired liver function. Z Ernahrungswiss 36, 364–367. [PubMed: 9467236]

Wan X, Xu C, Yu C, Li Y, 2016 Role of NLRP3 Inflammasome in the Progression of NAFLD to NASH. Can J Gastroenterol Hepatol 2016, 6489012. [PubMed: 27446858]

Wree A, McGeough MD, Pena CA, Schlattjan M, Li H, Inzaugarat ME, Messer K, Canbay A, Hoffman HM, Feldstein AE, 2014 NLRP3 inflammasome activation is required for fibrosis development in NAFLD. Journal of molecular medicine (Berlin, Germany) 92, 1069–1082.

Xing Y, Xu Y, Chen Y, Jeffrey PD, Chao Y, Lin Z, Li Z, Strack S, Stock JB, Shi Y, 2006 Structure of protein phosphatase 2A core enzyme bound to tumor-inducing toxins. Cell 127, 341–353. [PubMed: 17055435]

Yang Q, Vijayakumar A, Kahn BB, 2018 Metabolites as regulators of insulin sensitivity and metabolism. Nature reviews. Molecular cell biology 19, 654–672. [PubMed: 30104701]

Yang SJ, Lim Y, 2014 Resveratrol ameliorates hepatic metaflammation and inhibits NLRP3 inflammasome activation. Metabolism: clinical and experimental 63, 693–701. [PubMed: 24629563]

Zhang C, Wang N, Xu Y, Tan HY, Li S, Feng Y, 2018a Molecular Mechanisms Involved in Oxidative Stress-Associated Liver Injury Induced by Chinese Herbal Medicine: An Experimental Evidence-Based Literature Review and Network Pharmacology Study. International journal of molecular sciences 19.

Zhang Q, Qin W, Yang L, An J, Zhang X, Hong H, Xu L, Wang Y, 2018b Microcystis bloom containing microcystin-LR induces type 2 diabetes mellitus. Toxicology letters 294, 87–94. [PubMed: 29777831]

Zhou L, Yu H, Chen K, 2002 Relationship between microcystin in drinking water and colorectal cancer. Biomed Environ Sci 15, 166–171. [PubMed: 12244757]

Highlights

- Early exposure of microcystin primes mouse liver for hepatic inflammation in adulthood
- Early microcystin priming followed by high fat diet in adulthood exacerbates liver injury
- NLRP3 deletion in mice resists inflammatory and steatohepatitis like phenotype in the liver
- NLRP3 activation worsens outcome in insulin resistance and hepatic metabolism

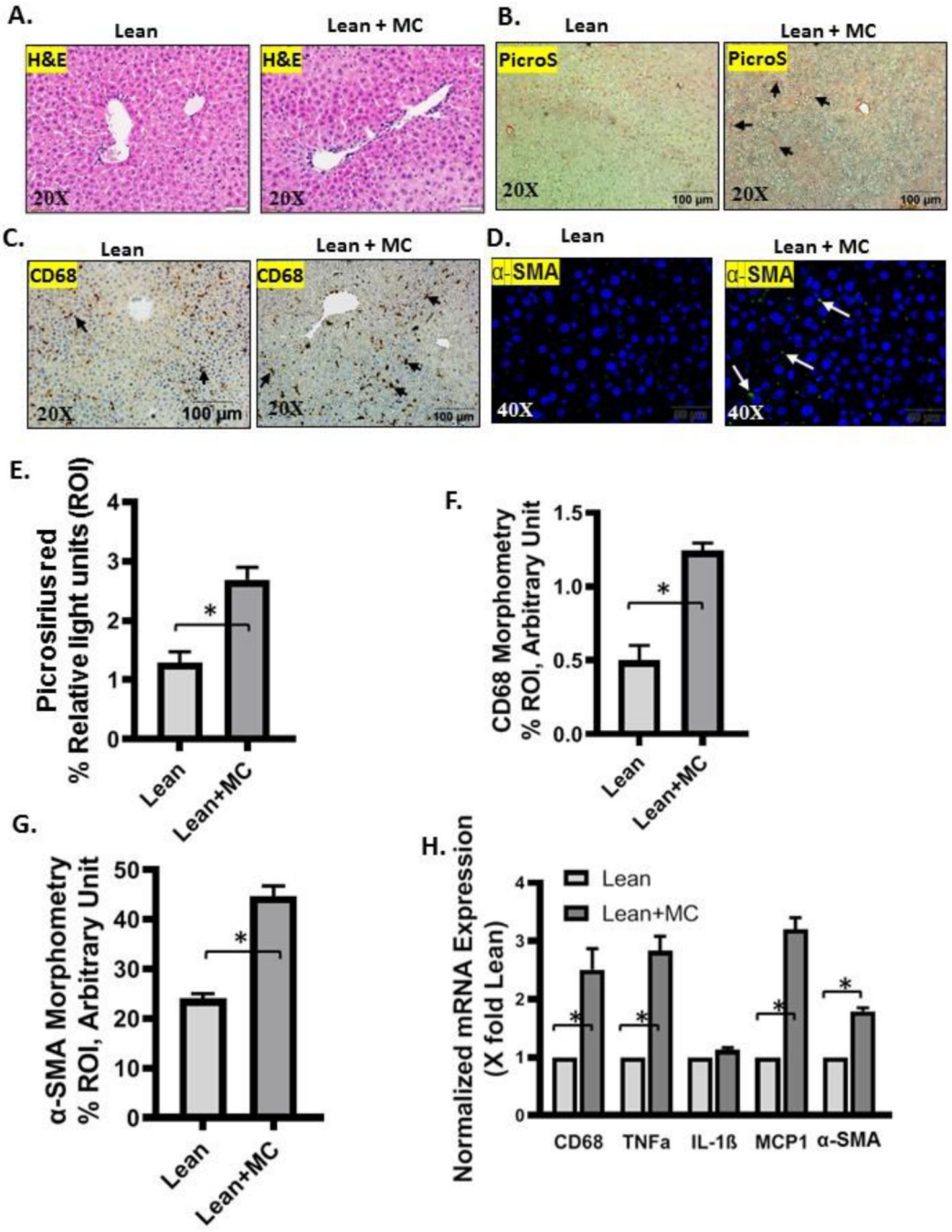

Fig. 1.

Liver pathology of early childhood exposure to MC-LR. Formailn-fixed, paraffin embedded 5 µm liver slices from lean mouse control (denoted as Lean) (n=3), and lean diet mouse exposed with MC-LR (Lean+MC) (n=3). A. Hematoxylin and eosin (H&E) staining of liver tissues indicated early hepatic injury in (Lean+MC) mice group when compared to Lean mice group. B. Picrosirius red staining (PicroS) showed mild fibrotic pathology in (Lean +MC) group compared to Lean mice group. C. Representative immunohistochemistry images of CD68 and D. immunofluorescence images stained with α-SMA (in Green) were

shown in Lean and microcystin exposed (Lean+MC) groups. 3–10 images were taken from the different microscopic field of each group and images were captured in 20X & 40X magnification. Immunoreactivity of CD68 and α-SMA was indicated by arrows. E. Morphometric analysis of picrosirius red staining estimated a significant increase of collagen fiber deposition in (Lean+MC) group of mice compared to Lean control group. ($p < 0.05$). Y-axis represents percentages of fibrosis expressed as %ROI. F. Morphometric analysis of CD68. Immunoreactivity of CD68 was expressed as %ROI along Y axis. G. α-SMA immunoreactivity expressed as %ROI showed a significant increase in (Lean+MC) group ($p < 0.05$). H. Normalized mRNA expression of CD68, TNF-α, MCP-1, α-SMA in Lean and (Lean+MC) group. The mRNA expressions were normalized with 18S and presented as fold change of Lean group. All data were represented as mean ± SEM. Significance was tested by performing unpaired t-test between Lean and (Lean+MC) groups (*$p < 0.05$), followed by Bonferroni Dunn Post hoc correction method.

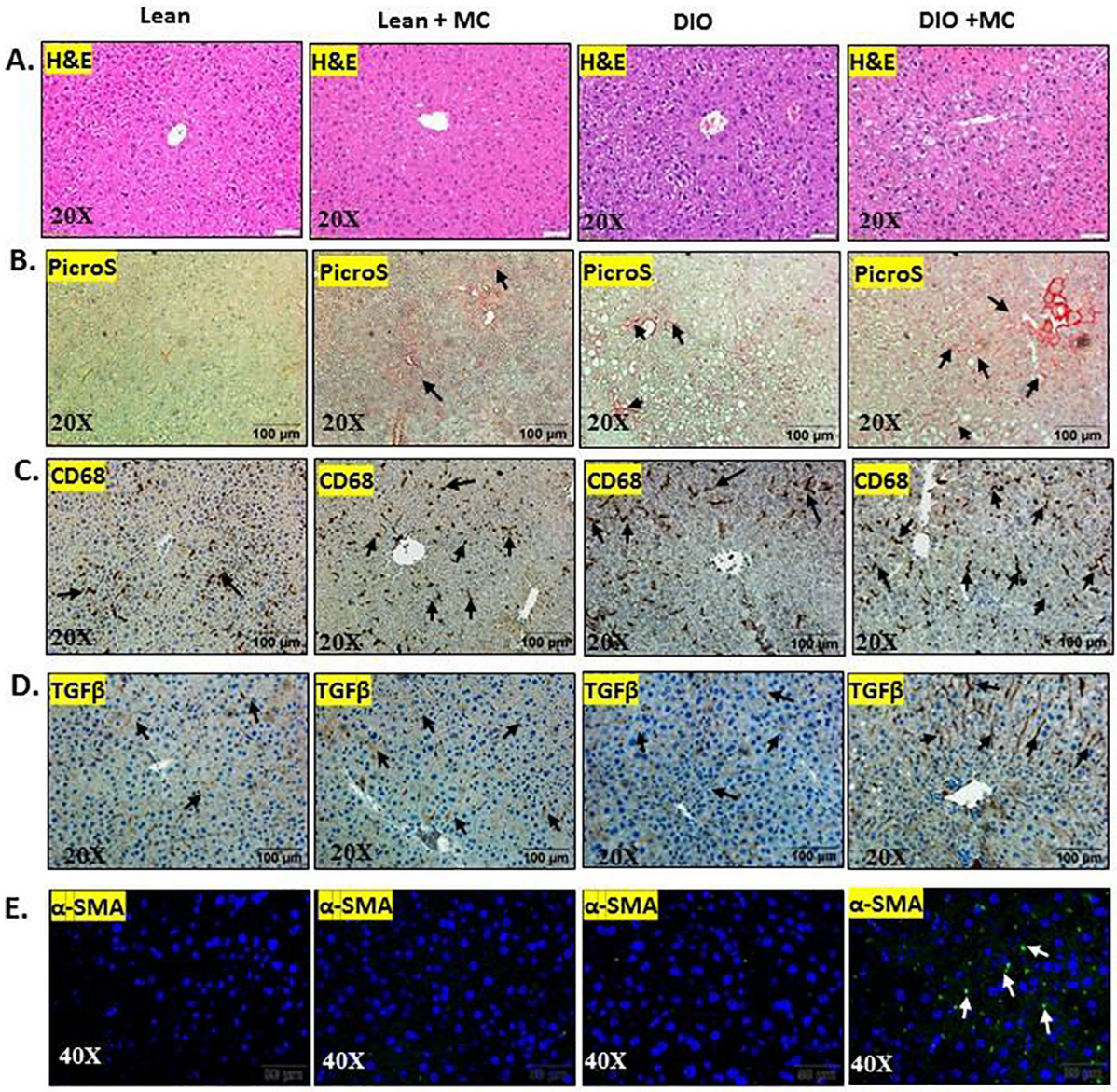

Fig. 2.

Liver pathology of early life exposure to MC-LR in diet induced obese mice. Formailn-fixed, paraffin embedded 5 μm liver slices from lean mouse control (Lean) (n=3), and lean diet mouse exposed with MC-LR (Lean+MC) (n=3), diet induced obese mice (DIO) (n=3), and diet induced obese mice exposed to MC-LR (DIO+MC) (n=3). A. Hematoxylin and eosin (H&E) stained images of liver tissues. Images were taken at 20X magnification. B. Picrosirius red staining (PicroS) images of liver tissues (20X). Collagen deposition in liver of MC-LR exposed groups were indicated by black arrows. Representative immunohistochemistry images (20X) depicting C. CD68, D. TGF-β immunoreactivity in liver. Immunoreactivity was indicated by black arrows. E. Immunofluorescence images of α-SMA (in green), counterstained with DAPI (blue). 3–10 images were taken from the different microscopic field of each group and images were captured in 40X magnification. Immunoreactivity was indicated by white arrows.

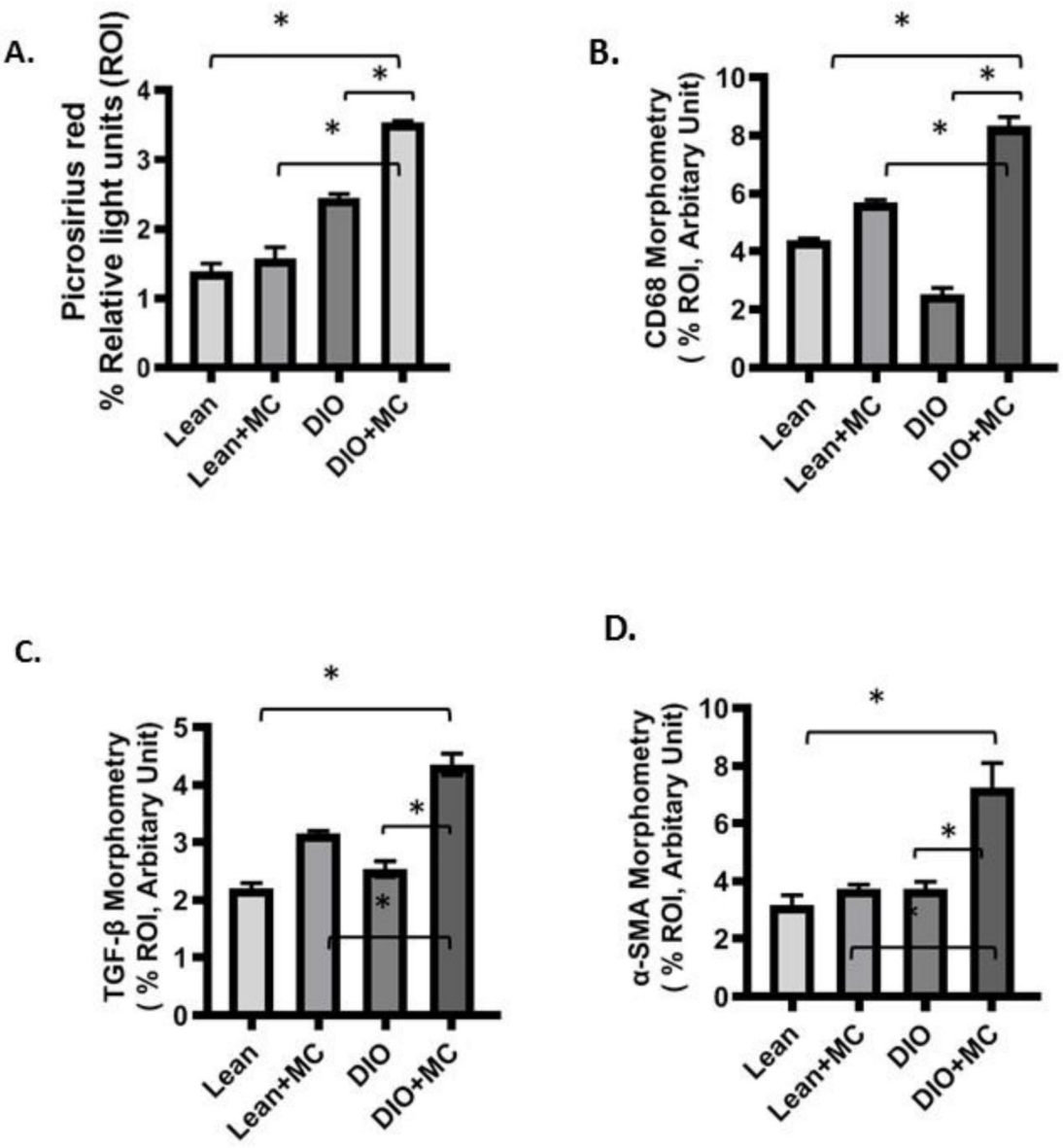

Fig. 3.

Morphometric analysis of A. picrosirius red staining images, Collagen fiber deposition was counted and indicated as %ROI along the Y-axis in Lean, (Lean+MC), DIO, (DIO+MC) groups. B. CD68, C. TGF-β, D. α-SMA immunoreactivity was plotted along Y-axis, calculated as %ROI. All data were represented as mean ± SEM. Significance was tested by performing unpaired t-test between (DIO+MC) and Lean, (DIO+MC) and (Lean+MC), (DIO+MC) and DIO groups (*p< 0.05), followed by Bonferroni Dunn Post hoc correction method.

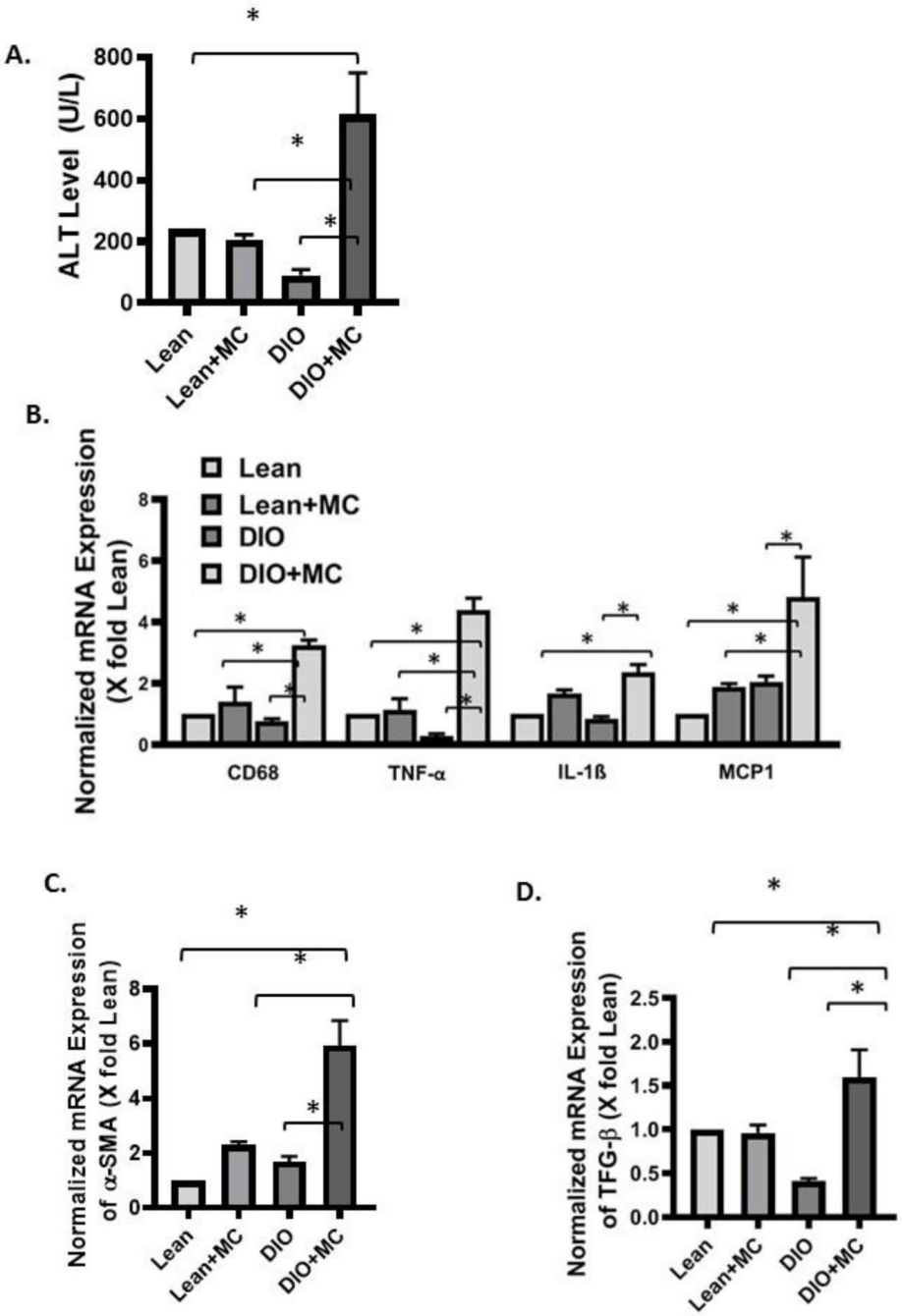

Fig. 4.

Early exposure to MC-LR followed by HFD causes an elevated serum ALT level and increased mRNA expression of Kuppfer cell biomarker, inflammatory cytokine, chemokine and fibrosis biomarkers. A. Serum ALT level was plotted as (U/L) against a bar graph. B. Normalized mRNA expression of CD68, TNF-α, IL-1β, MCP-1, C. α-SMA, D. TGF-β showed an increased level in the (DIO+MC) group compared to Lean, (Lean+MC) or DIO group (*p< 0.05). The mRNA expressions were normalized with 18S and presented as fold change of Lean group. All data were represented as mean ± SEM. Significance was tested

by performing unpaired t-test between (DIO+MC) and Lean, (DIO+MC) and (Lean+MC), (DIO+MC) and DIO groups (*p< 0.05), followed by Bonferroni Dunn Post hoc correction method.

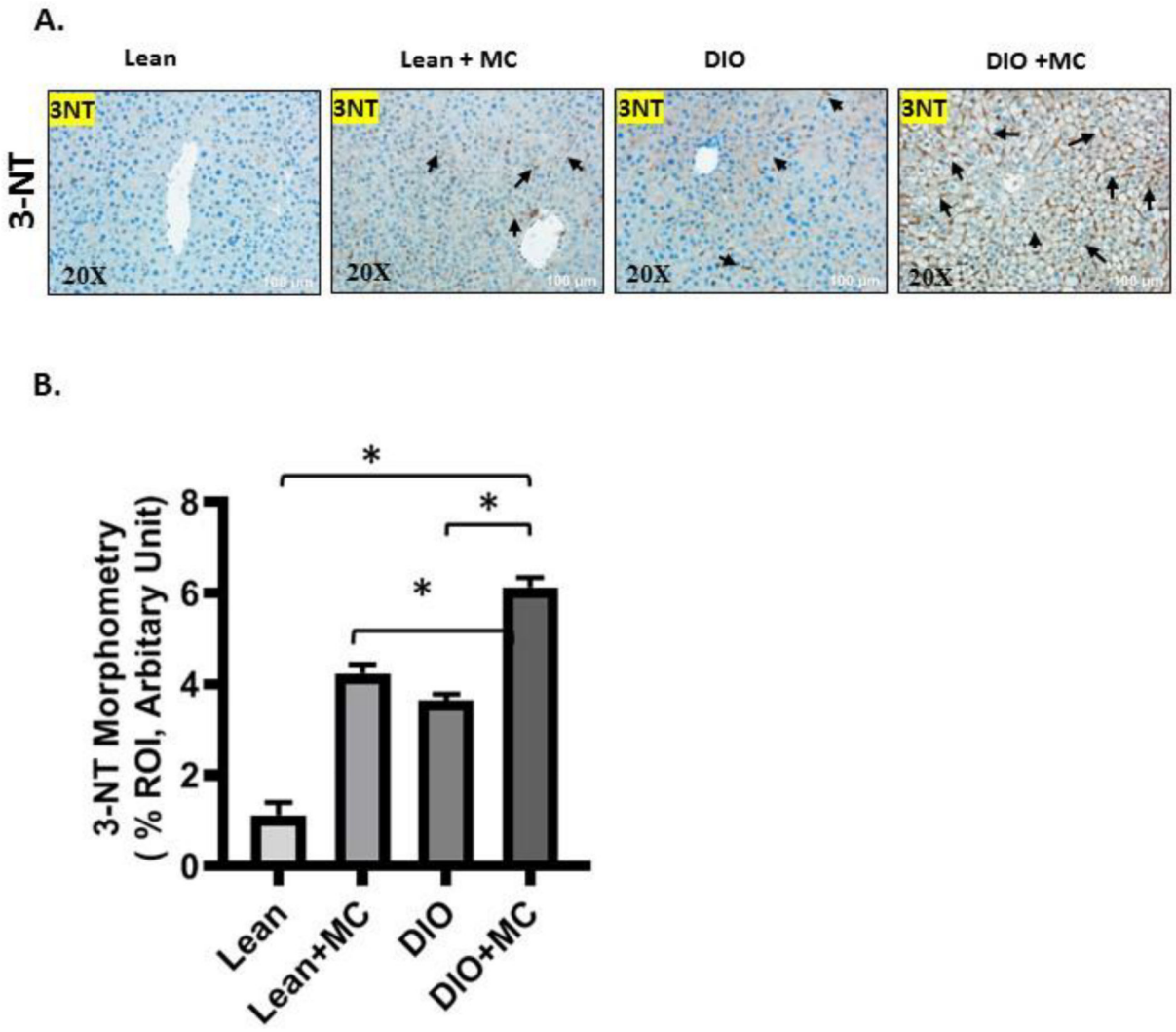

Fig. 5.

Early exposure to MC-LR followed by HFD leads to production of 3-nitrotyrosine in liver. A. Representative immunohistochemistry images of 3-NT immunoreactivity in Lean, (Lean +MC), DIO and (DIO+MC) groups. 3–10 images were taken from the different microscopic field of each group and images were captured in 20X magnification. Immunoreactivity was indicated by black arrows. B. Morphometric analysis (calculated as %ROI) of 3-NT denoted a significant increase in 3-NT formation. All data were represented as mean ± SEM. Significance was tested by performing unpaired t-test between (DIO+MC) and Lean, (DIO +MC) and (Lean+MC), (DIO+MC) and DIO groups (*p< 0.05), followed by Bonferroni Dunn Post hoc correction method.

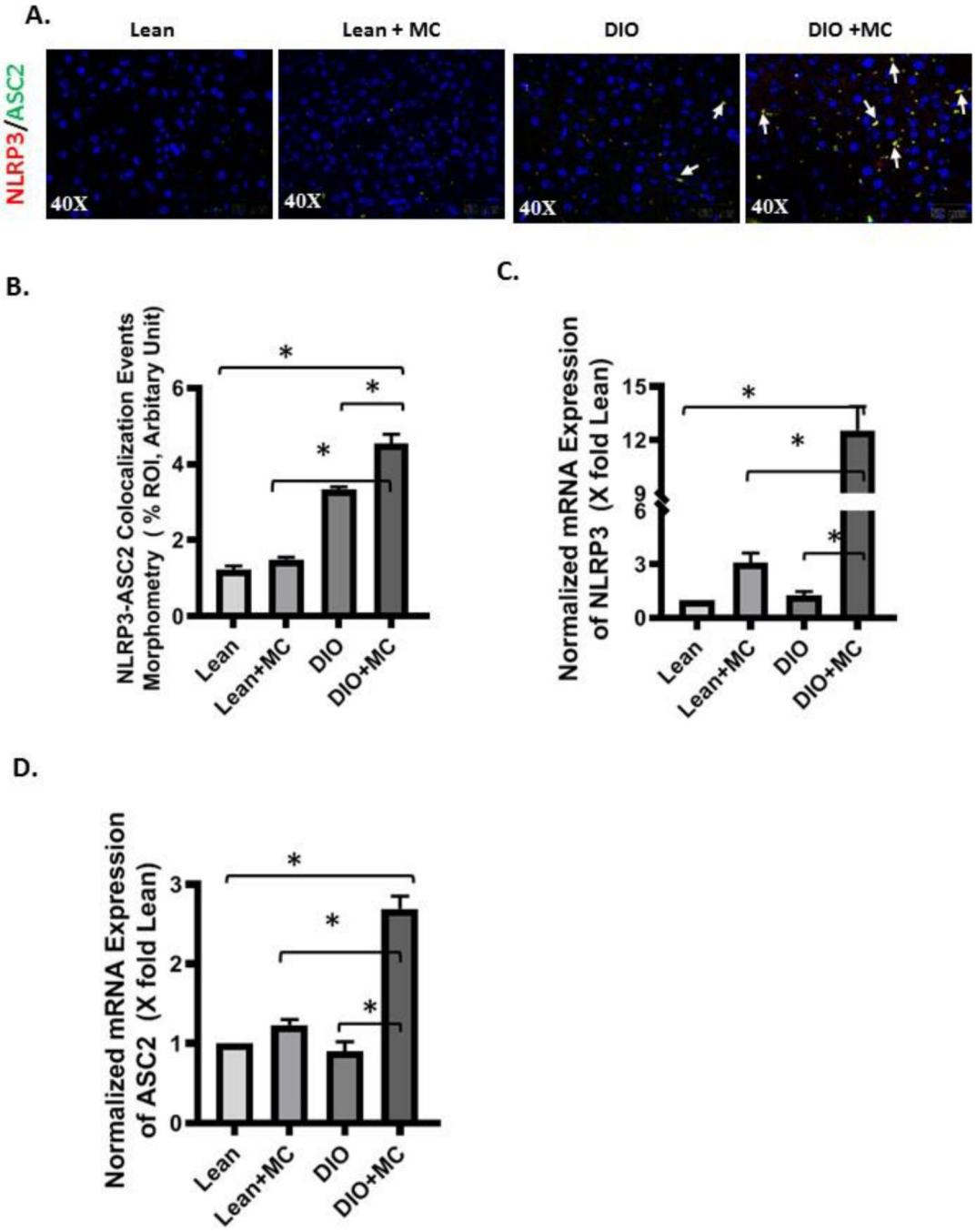

Fig. 6.

Early life MC-LR exposure and high fat diet activates hepatic NLRP3 inflammasome. A. Representative immunofluorescence images of NLRP3 (red) and ASC2 (green) co-localization event. The liver sections were counterstained with DAPI (blue). 3–10 images were taken from the different microscopic field of each group and images were captured in 40X magnification. Co-localization was represented by yellow dots. B. Morphometric analysis (calculated as %ROI) of NLRP3-ASC 2 co-localization was plotted on Y-axis against a bar graph. Normalized mRNA expression of C. NLRP3 and D. ASC2 in Lean,

(Lean+MC), DIO group and (DIO+MC) group. The mRNA expressions were normalized with 18S and presented as fold change of Lean group. All data were represented as mean ± SEM. Significance was tested by performing unpaired t-test between (DIO+MC) and Lean, (DIO+MC) and (Lean+MC), (DIO+MC) and DIO groups (*$p < 0.05$), followed by Bonferroni Dunn Post hoc correction method.

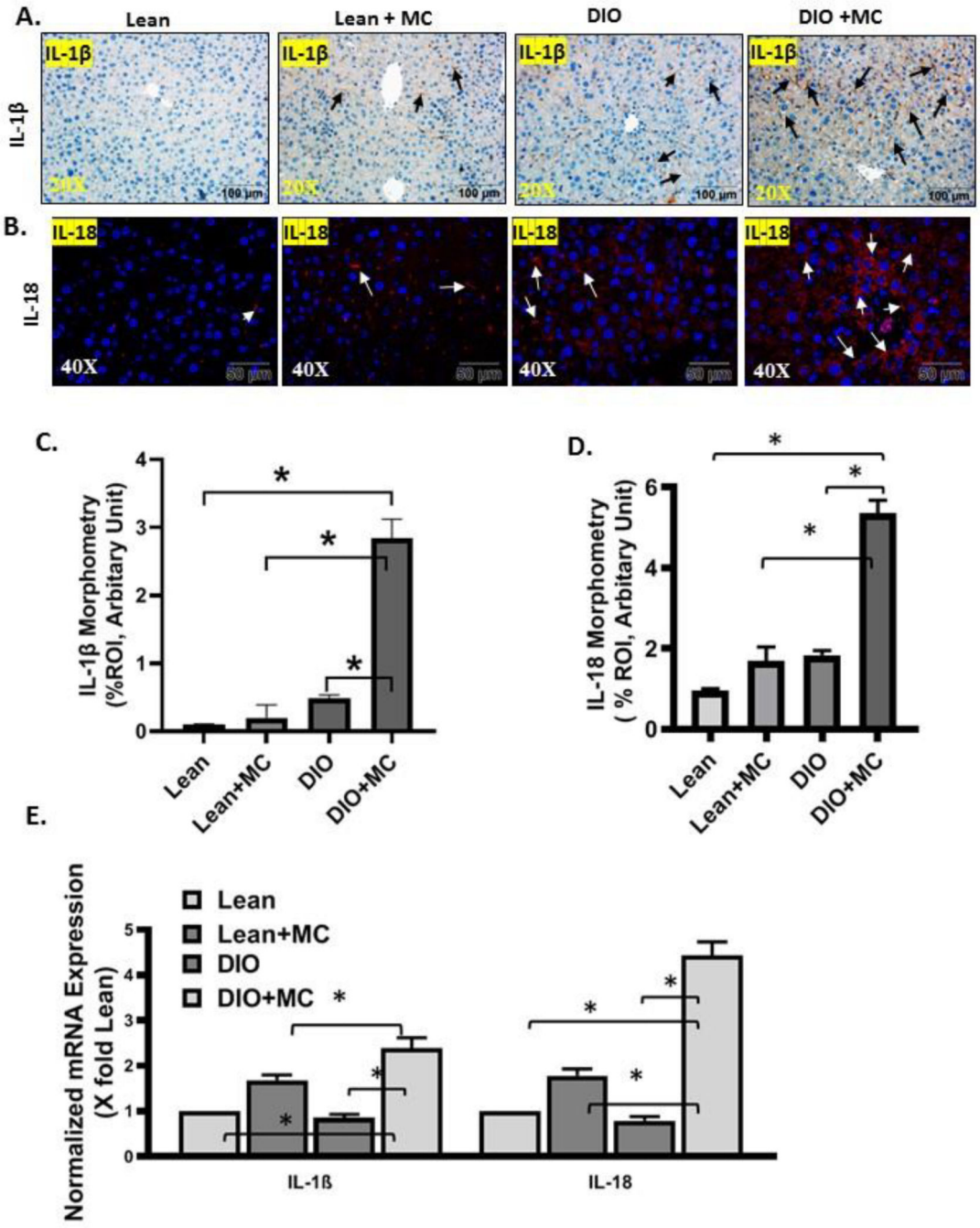

Fig. 7.

Early life MC-LR exposure and high fat diet induced hepatic NLRP3 inflammasome activation mediates release of inflammatory cytokines. Representative immunofluorescence images of A. IL-1β, and B. IL-18 (in red) immunoreactivity was observed in Lean, (Lean +MC), DIO & (DIO+MC) groups. The liver sections were counterstained with DAPI (blue). 3–10 images were taken from the different microscopic field of each group and images were captured in 40X magnification. Immunoreactivity was indicated by white arrows. Morphometric analysis (calculated as %ROI) of C. IL-1β & D. IL-18. in Lean, (Lean+MC),

DIO and (DIO+MC) groups. E. Normalized mRNA expression of IL-1β and IL-18 showed an increased level in the (DIO+MC) group compared to Lean, (Lean+MC) or DIO group ($p < 0.05$). The mRNA expressions were normalized with 18S and presented as fold change of Lean group. All data were represented as mean ± SEM. Significance was tested by performing unpaired t-test between (DIO+MC) and Lean, (DIO+MC) and (Lean+MC), (DIO+MC) and DIO groups (*$p < 0.05$), followed by Bonferroni Dunn Post hoc correction method.

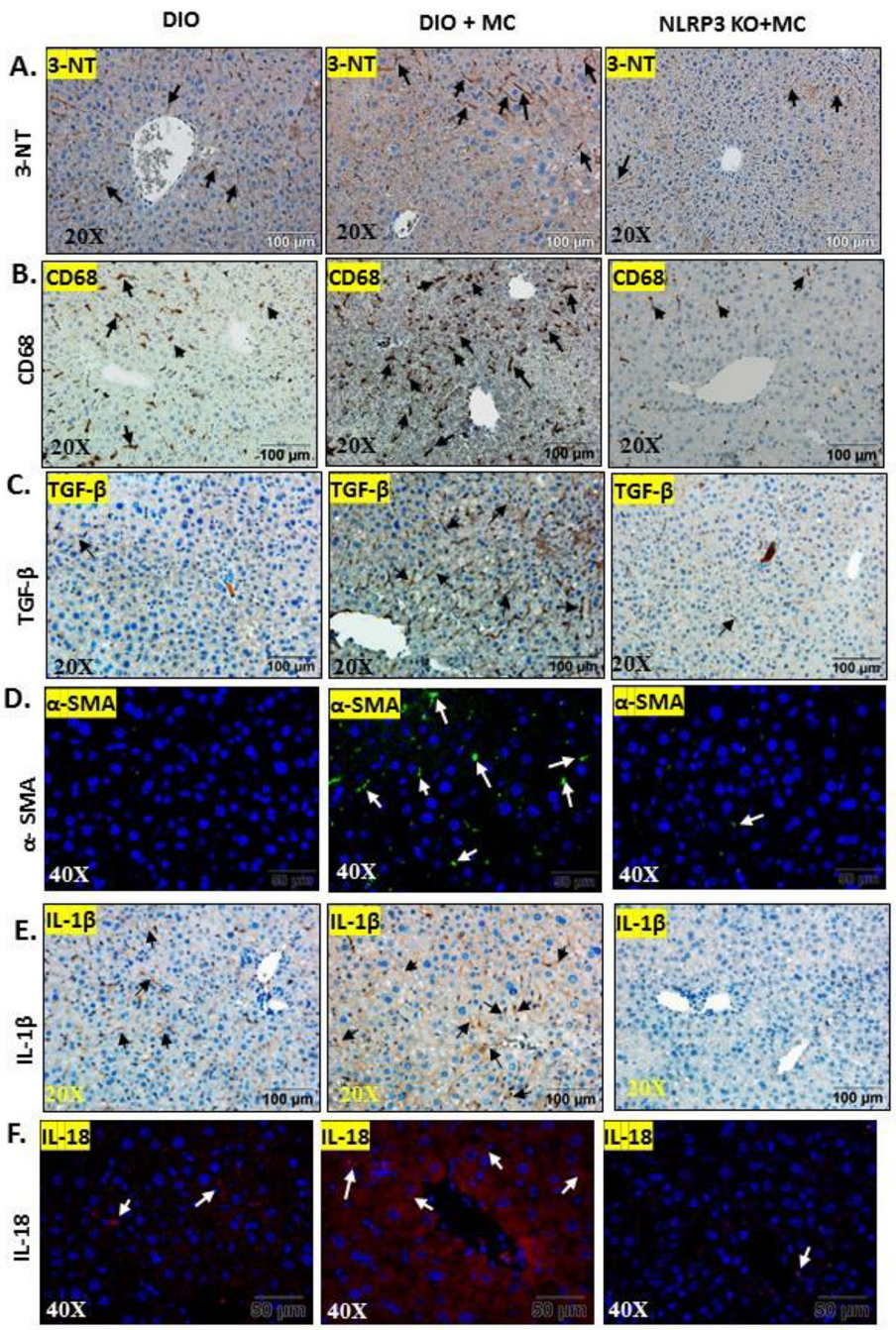

Fig. 8.

A consistent fat laden diet allows MC-LR induced inflammatory phenotype to persist via NLRP3 inflammasome activated pathway. Formailn-fixed, paraffin embedded 5 μm liver slices from diet induced obese mice (DIO) (n=3), diet induced obese mice exposed to MC-LR (DIO+MC) (n=3), and NLRP3 KO mice group exposed to MC-LR (NLRP3 KO+MC) (n=3). Representative immunohistochemistry images of A. 3-NT, B. CD68, C. TGF-β and immunofluorescence images of D. α-SMA (in green), E. IL-1β (in red), F. IL-18 (in red) immunoreactivity in DIO, (DIO+MC) and (NLRP3 KO+MC) groups. 3–10 images were

taken from the different microscopic field of each group and images were captured in 20X and 40X magnification. Immunoreactivity was indicated by black arrows in immunohistochemistry images and by white arrows in immunofluorescence images.

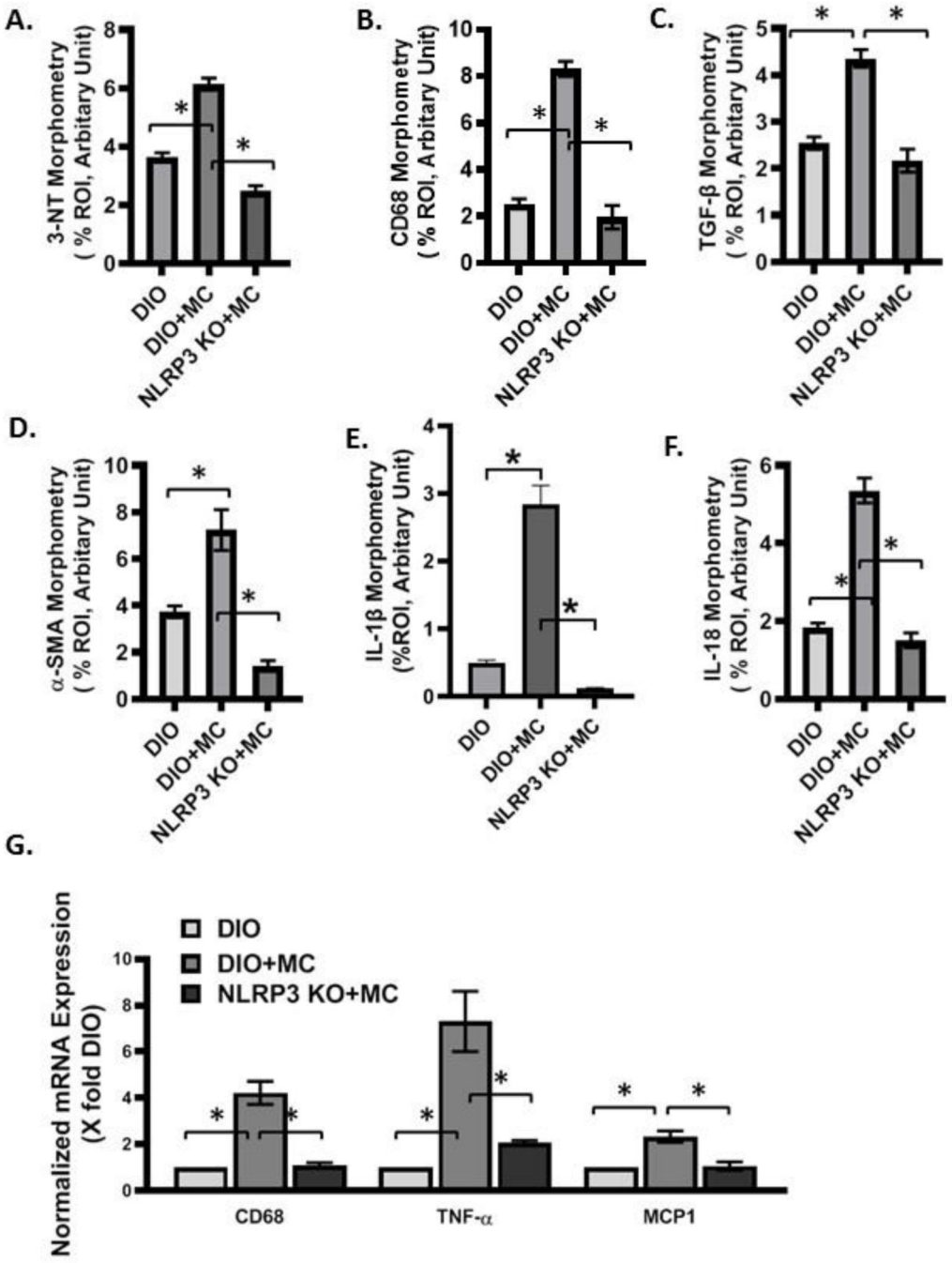

Fig. 9.

Morphometric analysis (calculated as %ROI) of A. 3-NT, B. CD68, C. TGF-β, D. α-SMA, E. IL-1β, F. IL-18 c. G. Normalized mRNA expression of CD68, TNF-α, IL-1β, MCP-1, in DIO, (DIO+MC) and (NLRP3 KO+MC) groups. The mRNA expressions were normalized with 18S and presented as fold change of DIO group. All data were represented as mean ± SEM. Significance was tested by performing unpaired t-test between (DIO+MC) and DIO groups and (DIO+MC) and (NLRP3 KO+MC) groups (*p< 0.05), followed by Bonferroni Dunn Post hoc correction method.

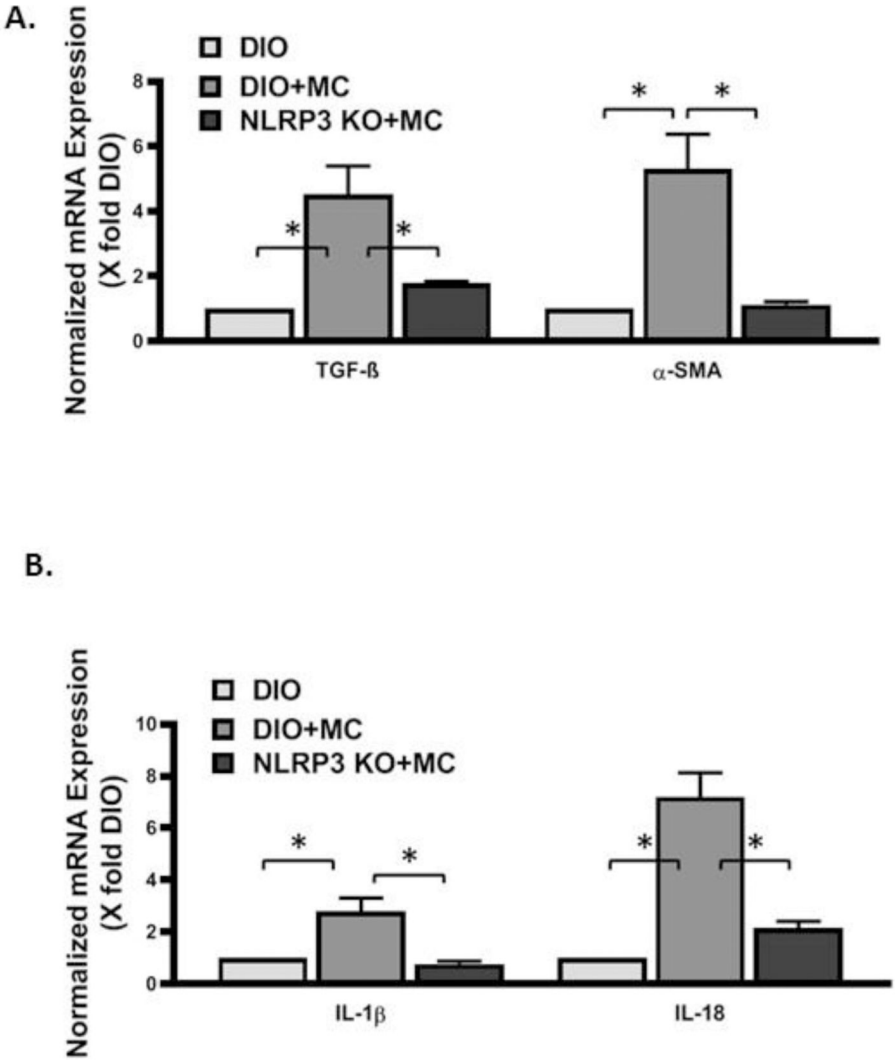

Fig. 10.

Normalized mRNA expression level of A. TGF-β, α-SMA, B. IL-1β and IL-18 in DIO, (DIO+MC) and (NLRP3 KO+MC) groups. The mRNA expressions were normalized with 18S and presented as fold change of DIO group. All data were represented as mean ± SEM. Significance was tested by performing unpaired t-test between (DIO+MC) and DIO groups and (DIO+MC) and (NLRP3 KO+MC) groups (*p< 0.05), followed by Bonferroni Dunn Post hoc correction method.

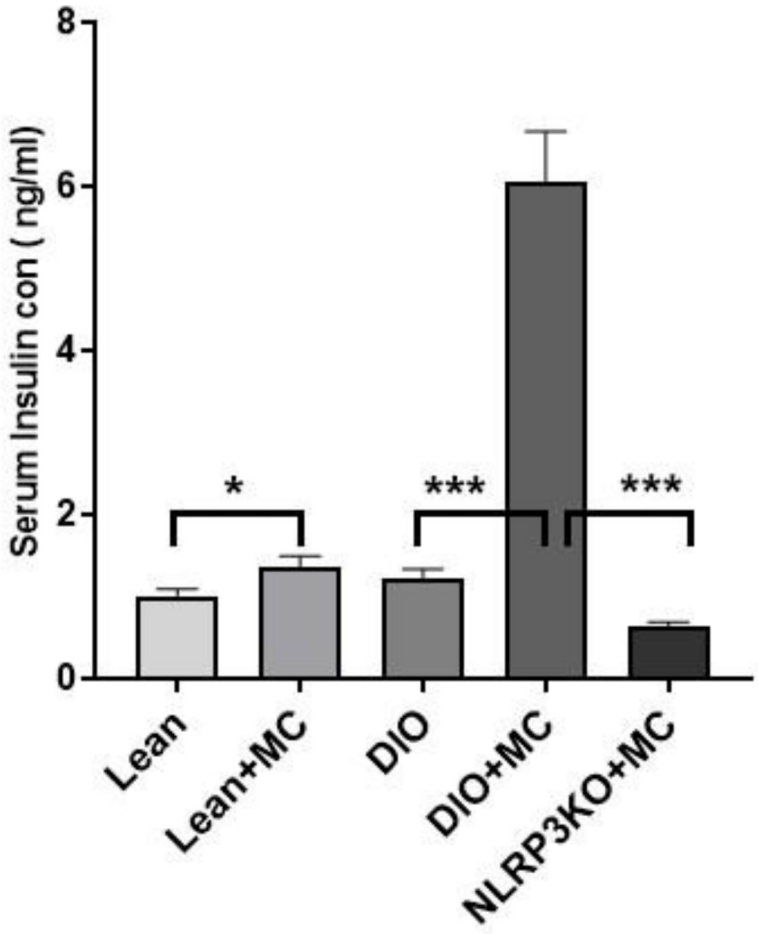

Fig. 11.

Serum insulin level was measured in Lean, (Lean+MC), DIO, (DIO+MC) and (NLRP3 KO +MC) (high fat diet and MC-LR exposed in NLRP3 KO mouse) groups. Serum insulin concentration (ng/ml) was plotted as bar graph. All data were represented as mean± SEM (n=3). Significance was tested by performing unpaired t-test between Lean and (Lean+MC) (*p< 0.05), DIO and (DIO+MC), (DIO+MC) and (NLRP3 KO+MC) ***p< 0.001), followed by Bonferroni Dunn Post hoc correction method.

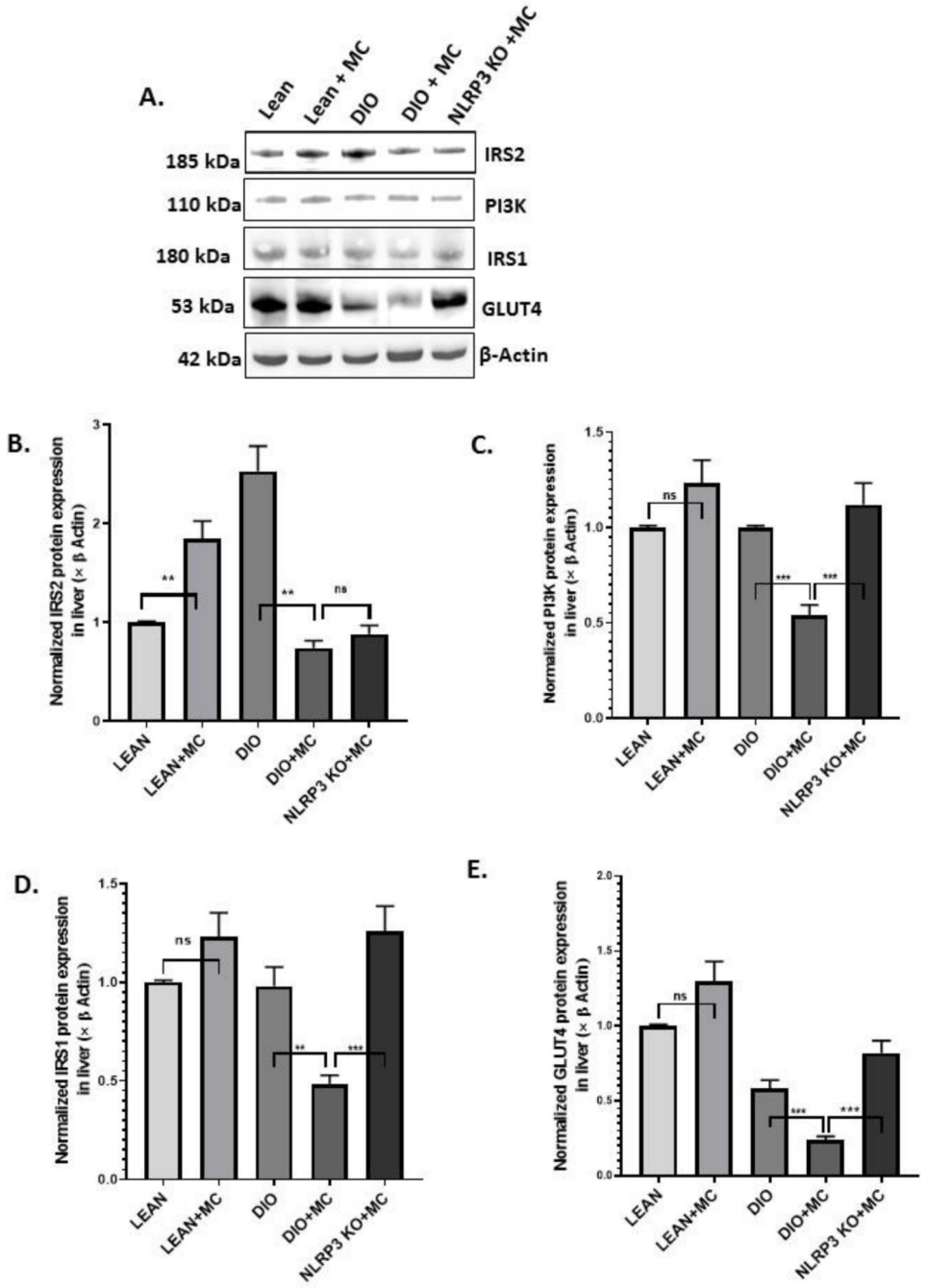

Fig. 12.

Western blot images of A. IRS2, PI3K, IRS1, GLUT4 protein expression level obtained from liver tissue lysates. (B-E) Densitometry analyses of immunoblots, displayed as mean± SEM and normalized against β-actin, were plotted as a bar graph. All data were represented as mean± SEM. Significance was tested by performing unpaired t-test between Lean and (Lean+MC), DIO and (DIO+MC), (DIO+MC) and (NLRP3 KO+MC). (*p< 0.05, **p< 0.01, ***p< 0.001, ns= non-significant), followed by Bonferroni Dunn Post hoc correction method.

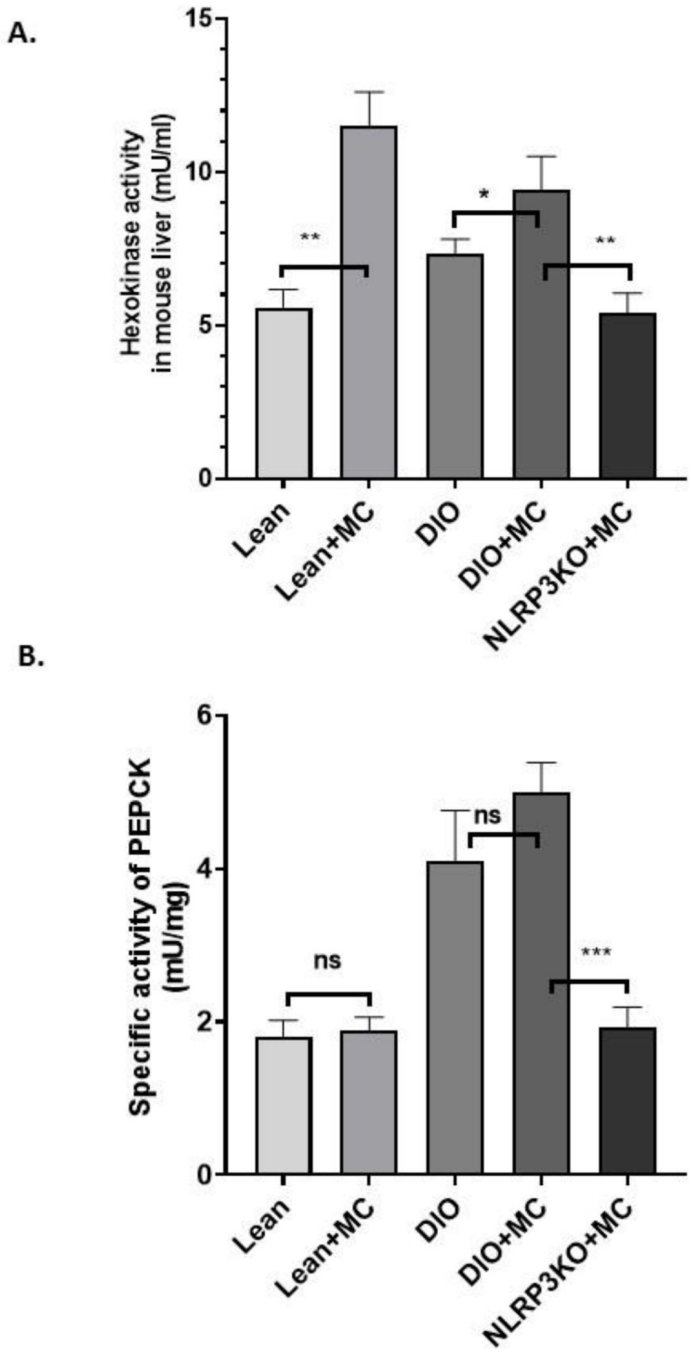

Fig. 13.

Early MC-LR priming and obese phenotype synergistically promote hepatic metabolic reprogramming. A. Intracellular HK activity and B. PEPCK specific activity obtained from the lean, (lean+MC), DIO, (DIO+MC), (NLRP3 KO+MC) groups. All data were represented as mean± SEM. Significance was tested by performing unpaired t-test between Lean and (Lean+MC), DIO and (DIO+MC), (DIO+MC) and (NLRP3 KO+MC). (*p< 0.05, **p<

0.01, ***p< 0.001, ns= non-significant), followed by Bonferroni Dunn Post hoc correction method.

Table 4.1.

Primer sequences for the different target genes.

Gene	Primer sequence
CD68 (Mouse)	Forward: GCTACATGGCGGTGGAGTACAA Reverse: ATGATGAGAGGCAGCAAGATGG
MCP-1 (Mouse)	Forward: CACAGTTGCCGGCTGGAGCAT Reverse: GTAGCAGCAGGTGAGTGGGGC
TNF-α (Mouse)	Sense: CAACGCCCTCCTGGCCAACG Antisense: TCGGGGCAGCCTTGTCCCTT
IL-1β (Mouse)	Sense: CCTCGGCCAAGACAGGTCGC Antisense: TGCCCATCAGAGGCAAGGAGGA
TGF-β (Mouse)	Sense: CTCACCGCGACTCCTGCTGC Antisense: TCGGAGAGCGGGAACCCTCG
α-SMA (Mouse)	Sense: GGAGAAGCCCAGCCAGTCGC Antisense: ACCATTGTCGCACACCAGGGC
NLRP3 (Mouse)	Sense: GGTGACCTTGTGTGTGCTTG Antisense: ATGTCCTGAGCCATGGAAGC
ASC-2 (Mouse)	Sense: GGACAGTACCAGGCAGTTCG Antisense: TTCTTGCAGGTCAGGTTCCA
IL-18 (Mouse)	Sense: ACACCACAAAACCTCAGCCA Antisense: AGGGACTTGAAACCAGAGCC